Simulating Lightning NO Production in CMAQv5.2: Performance Evaluations

Daiwen Kang[1]*, Kristen M. Foley[1], Rohit Mathur[1], Shawn J. Roselle[1], Kenneth E. Pickering[2], and Dale J. Allen[2]

[1]Center for Environmental Measurement & Modeling, U.S. Environmental Protection Agency, Research Triangle Park, NC 27711, USA

[2]Department of Atmospheric and Oceanic Science, University of Maryland, College Park, MD, USA

*Corresponding author: Daiwen Kang, US EPA, 109 T.W. Alexander Drive, Research Triangle Park, NC 27711, USA. Tel.: 919-541-4587; fax: 919-541-1379; e-mail: kang.daiwen@epa.gov

Abstract

This study assesses the impact of the lightning NO (LNO) production schemes in the Community Multiscale Air Quality (CMAQ) model on ground-level air quality as well as aloft atmospheric chemistry through detailed evaluation of model predictions of nitrogen oxides (NO_x) and ozone ($O_{3)}$ with corresponding observations for the U.S. For ground-level evaluations, hourly O_3 and NO_x from the US EPA's AQS monitoring network are used to assess the impact of different LNO schemes on model prediction of these species in time and space. Vertical evaluations are performed using ozonesonde and P-3B aircraft measurements during the DISCOVER-AQ campaign conducted in the Baltimore/Washington region during July 2011. The impact on wet deposition of nitrate is assessed using measurements from the National Atmospheric Deposition Program's National Trends Network (NADP/NTN). Compared with the base model (without LNO), the impact of LNO on surface O_3 varies from region to region depending on the base model conditions. Overall statistics suggest that for regions where surface O_3 mixing ratios are already overestimated, the incorporation of additional NO from lightning generally increased model overestimation of mean daily maximum 8-hr (DM8HR) O_3 by 1-2 ppb. In regions where surface O_3 is underestimated by the base model, LNO can significantly reduce the underestimation and bring model predictions close to observations. Analysis of vertical profiles reveals that LNO can significantly improve the vertical structure of modeled O_3 distributions by reducing underestimation aloft, and to a lesser degree decreasing overestimation near the surface. Since the base model underestimates the wet deposition of nitrate in most regions across the modeling domain except the Pacific Coast, the inclusion of LNO leads to reduction in biases and errors and an increase in correlation coefficients at almost all the NADP/NTN sites. Among the three LNO schemes described in Kang et al. (2019), the hNLDN scheme, which is implemented using hourly observed lightning flash data from National Lightning Detection Network (NLDN), performs best for the ground-level, vertical profiles, and wet deposition comparisons except that for the accumulated wet deposition of nitrate, the mNLDN scheme (the monthly NLDN-based scheme) performed slightly better. However, when observed lightning flash data are not available, the linear regression-based parameterization scheme, pNLDN, provides an improved estimate for nitrate wet deposition compared to the base simulation that does not include LNO.

1. Introduction

The potential importance of nitrogen oxides (NO_x; $NO_x = NO + NO_2$) produced by lightning (LNOx; due to the equilibrium coexistence of NO and NO_2 in the atmosphere, in the literature it is often collectively referred to as LNOx. However, the immediate release of lightning flashes is just NO, and the schemes in Kang et al., 2019 also generate NO emissions only, so in this paper it is primarily referred to as LNO) on regional air quality was recognized more than two decades ago (e.g. Novak and Pierce, 1993), but LNO emissions have only been added to regional chemistry and transport models during the last decade (e.g. Allen et al., 2012; Kaynak et al., 2008; Koshak et al., 2014; Smith and Mueller, 2010; Koo et al., 2010) owing in part to the limited understanding of this NO_x source (Schumann and Huntrieser, 2007; Murray, 2016; Pickering et al, 2016). As a result of efforts to reduce anthropogenic NOx emissions in recent decades (Simon et al., 2015; https://gispub.epa.gov/air/trendsreport/2018), it is expected that the relative contribution of LNO to the tropospheric NO_x burden and its subsequent impacts on atmospheric chemistry as one of the key precursors for ozone (O_3), hydroxyl radical (OH), nitrate, and other species will increase in the United States and other developed countries (Kang and Pickering, 2018). The significant impact of LNO on process-based understanding of surface air quality was earlier reported by Napelenok et al. (2008), which found low-biases in upper tropospheric NO_x in Community Multiscale Air Quality Model (CMAQ) (Byun and Schere, 2006) simulations without LNO emissions made it difficult to constrain ground-level NO_x emissions using inverse methods and Scanning Imaging Absorption Spectrometer for Atmospheric Cartography (SCIAMACHY) NO_2 retrievals (Bovensmann et al., 1999; Sioris et al., 2004; Richter et al., 2005). Appel et al. (2011) and Allen et al. (2012) reported that NO_3^- wet deposition at National Atmospheric Deposition Program (NADP) sites was underestimated by a factor of two when LNO was not included.

LNO production and distribution were parameterized initially in global models (e.g. Stockwell et al., 1999; Labrador et al., 2005) relying on the work of Price and Rind (1992) and Price et al. (1997) in that lightning flash frequency was parameterized as a function of the maximum cloud-top-height. Other approaches for LNO parameterization include a combination of latent heat release and cloud-top-height (Flatoy and Hov, 1997), convective precipitation rate (e.g. Allen and Pickering, 2002), convective available potential energy (Choi et al., 2005), or

convectively induced updraft velocity (Allen et al., 2000; Allen and Pickering, 2002). More recently, Finney et al. (2014, 2016) adopted a lightning parameterization using upward cloud ice flux at 440hPa (based upon definitions of deep convective clouds in the International Satellite Cloud Climatology Project (Rossow et al., 1996)) and implemented it in the United Kingdom Chemistry and Aerosol model (UKCA). With the availability of lightning flash data from the National Lightning Detection Network (NLDN) (Orville et al., 2002), recent LNO parameterization schemes started to include the observed lightning flash information to constrain LNO in regional Chemical Transport Models (CTMs) (Allen et al., 2012). In Kang et al. (2019), we described the existing LNO parameterization scheme that is based on the monthly NLDN (mNLND) lightning flash data, and an updated scheme using hourly NLDN (hNLDN) lightning flash data in the CMAQ lightning module. In addition, we also developed a scheme based on linear and log-linear regression parameters using multiyear NLDN observed lightning flashes and model predicted convective precipitation rate (pNLDN). The preliminary assessment of these schemes based on total column LNO suggests that all the schemes provide reasonable LNO estimates in time and space, but during summer months, the mNLDN scheme tends to produce the most and the pNLDN scheme the least LNO.

The first study on the impact of LNO on surface air quality using CMAQ was conducted by Allen et al. (2012) and followed by Wang et al. (2013) with different ways for parameterizing LNO production and different model configurations. In this study, we present performance evaluations using each of the LNO production schemes (mNLDN, hNLDN, pNLDN) described by Kang et al. (2019) to provide estimates of LNO in CMAQ. In addition to examination of differences in air quality estimates between these schemes, we compare the model predictions to base model estimates without LNO and evaluate the estimates from all of the simulations against surface and airborne observations.

Section 2 describes the model configuration, simulation scenarios, analysis methodology, and observational data. Section 3 presents the analysis results and Section 4 presents the conclusions.

2. Methodology

2.1 The LNO schemes

In air quality models, three steps are involved in generating LNO emissions: (1) identify lightning flashes, (2) produce the total column NO at model grid cells, and (3) distribute the column NO into model layers vertically. Three schemes to produce total column LNO emissions are examined in this study: mNLDN – based on monthly mean NLDN lightning flashes and convective precipitation predicted by the upstream meteorological model, hNLDN – directly use the observed NLDN lightning flashes that are aggregated into hourly values and gridded onto model grid cells, and pNLDN – a linear and log-linear regression parameterization scheme derived using multiyear observed lightning flash rate and model predicted convective precipitation. After total column LNO is produced at model grid cells, it is distributed onto vertical model layers using the double-peak vertical distribution algorithm described in Kang et al. (2019), which also provides detailed description and formulation of all the LNO schemes.

2.2 The CMAQ model and simulation configurations

The CMAQ model (Appel et al. 2017) version 5.2 were configured with the CB6 chemical mechanism (Yarwood et al., 2010) and the AERO6 aerosol module (Nolte et al., 2015). The meteorological inputs were provided by the Weather Research and Forecasting (WRF) model version 3.8 and the model-ready meteorological input files were created using version 4.2 of the meteorology–chemistry interface processor (MCIP; Otte and Pleim, 2010).

The modeling domain covers the entire contiguous United States (CONUS) and surrounding portions of northern Mexico and southern Canada, as well as the eastern Pacific and western Atlantic oceans. The model domain consists of 299 north–south grid cells by 459 east–west grid cells utilizing 12 km x 12 km horizontal grid spacing, 35 vertical layers with varying thickness extending from the surface to 50 hPa and an approximately 10 m midpoint for the lowest (surface) model layer. The simulation time period covers the months from April to September 2011 with a 10-day spin-up period in March.

Emission input data were based on the 2011 National Emissions Inventory (https://www.epa.gov/air-emissions-inventories). The raw emission files were processed using

version 3.6.5 of the Sparse Matrix Operator Kernel Emissions (SMOKE; https://www.cmascenter.org/smoke/) processor to create gridded speciated hourly model-ready input emission fields for input to CMAQ. Electric generating unit (EGU) emissions were obtained using data from EGUs equipped with a continuous emission monitoring system (CEMS). Plume rise for point and fire sources were calculated in-line for all simulations (Foley et al., 2010). Biogenic emissions were generated in-line in CMAQ using BEIS versions 3.61 (Bash et al., 2016). All the simulations employed the bidirectional (bi-di) ammonia flux option for estimating the air-surface exchange of ammonia.

There are four CMAQ simulation scenarios for this study: 1) simulation without LNO (Base), 2) simulation with LNO generated by the scheme based on monthly information from the NLDN (mNLDN), 3) simulation with LNO generated by scheme based on hourly information from the NLDN (hNLDN), and 4) simulation with LNO generated by the scheme parameterizing lightning emissions based on modeled convective activity (pNLDN) as described in detail in Kang et al. (2019). All other model inputs, parameters and settings were the same across the four simulations. The vertical distribution algorithm is the same for all the LNO schemes as also described in Kang et al. (2019).

2.3 Observations and analysis techniques

To assess the impact of LNO on ground-level air quality, output from the various CMAQ simulations were paired in space and time with observed data from the EPA's Air Quality System (AQS; https://www.epa.gov/aqs) for hourly O_3 and NO_x. To evaluate the vertical distribution, measurements of trace species from the Deriving Information on Surface Conditions from Column and Vertically Resolved Observations Relevant to Air Quality (DISCOVER-AQ; http://www.nasa.gov/missions/discover-aq) campaign conducted in the Baltimore/Washington region (e.g., Crawford and Pickering, 2014; Anderson et al., 2014; Follette-Cook et al., 2015) were used. During this campaign, the NASA P-3B aircraft measured trace gases including O_3, NO, and NO_2. Vertical profiles were obtained over seven locations – Beltsville (Be), Padonia (Pa), Fairhill (Fa), Aldino (Al), Edgewood (Ed), Essex (Es), and Chesapeake Bay (Cb) from approximately 0.3 to 5 km above ground level during P-3B flights over 14 days in July 2011. During this same period, ozonesonde measurements were taken that extended from ground level through the entire model column at two locations (Beltsville, MD and Edgewood, MD shown in

Figure 1). Inclusion of LNO estimates in the CTM simulations also has an important impact on model estimated wet deposition of nitrate. Therefore, assessment was also performed using data from the National Atmospheric Deposition Program's National Trends Network (NADP/NTN, http://ndp.slh.wisc.edu/ntn).

Since lightning activity as well as LNO exhibit distinct spatial variations (Kang and Pickering, 2018), analysis was conducted for the model domain over the contiguous United States, and then for each region as shown in Figure 1. Emphasis is placed on two regions, Southeast (SE) and Rocky Mountains (RM), where lightning activity is more prevalent and LNO has the greatest impact on model predictions as shown in Results - increasing model bias in the SE and decreasing bias in the RM. The commonly used statistical metrics, Root Mean Square Error (RMSE), Normalized Mean Error (NME), Mean Bias (MB), Normalized Mean Bias (NMB), and Correlation Coefficient (R), in the model evaluation field as defined in Kang et al. (2005) and Eder et al. (2006) were calculated to assess the basic performance differences among all the model cases for their ground-level air quality predictions.

3. Results

3.1 Ground-level evaluation for O_3 and NO_x

3.1.1 Statistical performance metrics

Tables 1 and 2 display the statistical model performance metrics for daily maximum 8-hr (DM8HR) O_3 and daily mean NO_x mixing ratios over the domain and each analysis region for all four model cases in July 2011 (Base, mNLDN, hNLDN, and pNLDN). The best performance metrics among the model cases are highlighted in bold. As shown in Table 1, for DM8HR O_3, the Base simulation has the lowest MB and NMB values over the Domain, while hNLDN produced the smallest RMSE and NME values. mNLDN generated the largest values for both error (RMSE and NME) and biases (MB and NMB), followed by pNLDN, and all model cases with LNO exhibit slightly higher correlation coefficients than the Base simulation. Additionally, the hNLDN simulation exhibited higher correlation and lower bias and error relative to the measurements indicating the value of higher temporal resolution lightning activity for representing the associated NO_x emissions and their impacts on tropospheric chemistry.

Examining the regional results for DM8HR O_3 in Table 1, the statistical measures indicate that in the Northeast (NE), hNLDN outperformed all other model cases with the lowest errors and biases and highest correlation coefficient. In Southeast (SE), the Base performed better with the lowest errors and mean biases, but the correlation coefficient (R) value for hNLDN is slightly higher. Among all the LNO cases, mNLDN produced the worst statistics in this region. Historically, CTMs tend to significantly overestimate surface O_3 in the Southeast US (Lin et al., 2008; Fiore et al., 2009; Brown-Steiner et al., 2015; Canty et al., 2015), and this is partially driven by a likely overestimation of anthropogenic NO_x emissions (Anderson et al., 2014). Thus, even though lightning is known to impact ambient air quality, including this additional NO_x source can worsen biases in model O_3 in some locations and time periods due to other errors in the modeling system. As noted in Table 1, for the SE, the MB values increased by about 1.6 ppb in mNLDN and less than 1 ppb in hNLDN and pNLDN. Nevertheless, the correlation coefficients for mNLDN and pNLDN are almost the same with the Base, and hNLDN was slightly higher (0.77 compared to 0.76). These correlations indicate that even though additional NO_x increases the mean bias, when it is added correctly in time and space, as with the case of hNLDN, the spatial and temporal correlation are slightly improved. In the Upper Midwest (UM), the lowest errors and biases among the model cases are associated with hNLDN, while the worst performance is with mNLDN. In the Lower Midwest (LM), hNLDN performed comparable with the Base, with hNLDN having the highest correlation and lowest mean errors, while the Base has the lowest mean biases. Rocky Mountain (RM) is the only region that shows an underestimation of DM8HR O_3. In this region all the model cases with LNO outperformed the Base case in all the metrics. Among the three model cases with LNO, mNLDN produced the lowest MB and NMB values, while hNLDN had the lowest RMSE and NME, and the highest correlation. In the Pacific Coast (PC) region, lightning activity is generally very low compared to other regions (Kang and Pickering, 2018). All model cases with LNO outperformed the Base case, especially hNLDN which had the lowest mean error and bias and highest correlation among all the cases.

Most of the NO_x produced by lightning is distributed in the middle and upper troposphere with only a small portion being distributed close to the surface. As a result, the impact on ground-level NO_x mixing ratios is small. Table 2 shows all the model cases produced similar statistics for the daily mean NO_x mixing ratios at AQS sites across the domain and within all the

subregions. Although the changes in model performance are small, the model cases with LNO exhibit similar or slightly better performance than the Base case.

3.1.2 Time series

Figure 2 presents timeseries of regional-mean observed and modeled DM8HR O_3 for the entire domain and the SE and RM regions during July 2011. Over the domain and in SE, all the model cases overestimate the mean DM8HR O_3 mixing ratios on all days with the Base being the closest to the observations. hNLDN is almost the same as the Base with slightly higher values on some days. Among all the cases, mNLDN produced the highest values on almost all days through the month, on the order of 1-2 ppb higher than the Base. In contrast, in the RM region, the Base significantly underestimates DM8HR O_3 mixing rations on all the days during the month, while all model cases with LNO improved model predictions relative to observations in the region. Among the three model cases with LNO, mNLDN produced the lowest bias for all the days, closely followed by hNLDN.

Figure 3 displays the average daily mean NO_x mixing ratios at AQS sites over the same regions as in Figure 2. On most of the days in July 2011, over the domain and in the SE, the model overestimate NO_x values, and on almost half of the days, the overestimation is significant (up to 100 %). As noted in Table 2, on average, the overestimation is ~17 % over the domain and ~43 % in SE. However, in RM, the predicted NO_x mixing ratios closely follow the daily observations and on average the modeled and observed magnitude is almost identical (~3 % difference). All the model cases, with or without LNO, produced almost the same mean NO_x mixing ratios at the surface. However, the different cases produce different levels of LNO in the middle and upper troposphere, resulting in differences in O_3 production and transport which impact radiative forcing and also downwind ground-level O_3 levels. We further explore these features in Section 3.2 which presents evaluation of modeled vertical pollutant distributions.

3.1.3 Diurnal variations

Diurnal plots are used to further examine differences in model evaluation for O_3 and NO_x. Figure 4 shows the mean diurnal profiles for hourly O_3 and NO_x over the entire domain, SE, and RM. On a domain mean basis, all model cases overestimate O_3 during the daytime hours, while in the SE, the overestimation spans all the hours. In RM, the model cases

significantly underestimate O_3 across all the hours except for a few early morning hours, when the model predicted values are very close to the observations. Among all the model cases, as expected, the most prominent differences occurred during the midday hours when the photochemistry is most active. However, the difference between hNLDN (and mNLDN) and the Base is also significant during the night in the RM region, even though the O_3 levels are low. This may be attributed to NO_x-related nighttime chemistry in part caused by freshly released NO by cloud-to-ground lightning flashes. The diurnal variations of NO_x are similar over the domain and in the regions for all model cases. Appel et al. (2017) reported a significant overestimation of NO_x mixing ratios at AQS sites during nighttime hours and underestimation during daytime hours. The bias pattern is identical for all of the LNO model cases evaluated here (Figure 4).

3.1.4 Spatial variations

Figure 5 shows the impact of the different LNO schemes on model performance for DM8HR O_3 at AQS sites. The spatial maps show the difference in absolute MB between the cases with lightning NO_x emissions and the Base and is calculated as follows. First, the absolute MB was calculated at each site for each case, e.g. $|MB_{[Base - Obs]}|$, then the difference in absolute MB was calculated between model cases, e.g. $|MB_{[hNLDN-Obs]}| - |MB_{[Base - Obs]}|$. The histograms of the differences in absolute MB between model cases in Figure 5 are provided to show the distribution of the change in model performance across space, i.e. the frequency of an improvement in model performance versus a degradation in model performance between cases. As shown in Figure 5, the mNLDN shows increased model bias in the east US and along the California coast, but reduced model bias in the RM. At a majority of the AQS sites, it increases the model bias (only decreases at 26.8 % (346) of the sites). The hNLDN also significantly reduces model bias in the RM with a moderate increase in the SE. Overall, in the hNLDN, the mean bias decreased at 61.2 % (791) of AQS sites. Similar to mNLDN, increases in mean bias are noted at 29.3 % (378) of the AQS sites in the pNLDN simulation. As noted in the histograms, the distribution of the model bias in the pNLDN is much narrower than both mNLDN and hNLDN, eliminating the large bias increases in mNLDN and the significant bias decreases in hNLDN.

3.2 Vertical evaluation for O_3 and NO_x

3.2.1 Ozone-sonde observations

A large source of uncertainty in the specification of LNO is its vertical allocation, which can impact the model's ability to accurately represent the variability in both chemistry and transport. To further assess the impact of the vertical LNO specification on model results, we compared vertical profiles of simulated model O_3 with extensive ozonesonde measurements available during the study period. Figure 6 presents the vertical profiles for O_3 sonde measurements and paired model estimates of all model cases at Beltsville, MD and Edgewood, MD. At each location, observations from multiple days are available (one or two soundings per day) during the 2011 DISCOVER-AQ campaign in July 2011. The model evaluation was limited to days where the inclusion of LNO has an obvious impact (the mean vertical profiles of LNO cases are separable from that of the base case) on the model estimates (July 21, 22, 28 and 29 at Beltsville, and July 21, 22, 28, 29, and 30 at Edgewood). We paired the observed data with model estimates in time and space and averaged the model and observed values at each model layer. Only data below 12 km altitude are plotted in Figure 6 to exclude possible influence of stratospheric air on O_3. As can be seen in Figure 6, at both locations the Base case underestimates O_3 mixing ratios above about 1 km, but overestimates values closer to the surface. When LNO is included in the simulations, the predicted O_3 mixing ratios increase relative to the Base case starting around 2km, with greater divergence from the Base case at higher altitudes. The two model cases, hNLDN and mNLDN, produced similar O_3 levels from the surface to about 6 km, but above that altitude the mNLDN ozone mixing ratios were higher. All the model cases with LNO performed much better aloft than the Base case. Near the surface, all the model cases overestimated O_3, however hNLDN had smaller bias than the other simulations. This may be attributed to the fact that only hNLDN used the observed lightning flash data directly, and as a result, LNO was estimated more accurately in time and space. This improvement in model bias at the surface is further investigated in the next section using evaluation against P-3B measurements.

3.2.2 P-3B measurement

Extensive measurements of lower tropospheric chemical composition distributions over the Northeastern U.S. are available from instruments onboard the P-3B aircraft on 14 days of the DISCOVER-AQ campaign. We utilize measurements from one of the days (28 July 2011) with

noticeable (the mean vertical profiles of LNO cases are separable from that of the base case) lightning impacts, to evaluate the model simulations. Figure 7 shows measured O_3 mixing ratios overlaid on the modeled vertical time-section for 1030 – 1730 UTC. The color-filled circles represent measured O_3 mixing ratios averaged over 60 seconds and the background is the model estimated vertical profiles from the grid cells containing the P-3B flight path for that hour and location. As indicated in the Base case (Figure 7a), the model tends to overestimate O_3 mixing ratios from the surface to about 2 km, but underestimate at altitudes above 2 km. The hNLDN reduced the overestimation below 2km, e.g. fewer grid cells with mixing ratios above 90ppb (shown in red). The other two cases (mNLDN, pNLDN) did not produce the same improvement near the surface. The hNLDN also decreases the underestimation aloft compared to the Base case with O_3 mixing ratios in the 55-65 ppb range (light blue colors), better matching the measured values. This decrease in underestimation aloft is also seen in the mNLDN case, but to a lesser degree while the pNLDN case shows only slight improvement aloft over the Base simulation.

To further differentiate the three LNO model cases, Figures 8-10 show the difference in the time-sections between each of the model cases with LNO and the Base for NO, NO_x, and O_3 from all the model layers along the P-3B flight path on July 28. As seen in Figure 8, the hNLDN scheme injected most NO above 5 km with a peak between 13-14 km and only a small amount near the surface. After release into the atmosphere, NO is quickly converted into NO_2 in the presence of O_3, and these collectively result in the NO_x vertical time-section (local production plus transport) shown in the middle panel of Figure 8. NO_x is further mixed down through the time-section and more persistent along the flight path near the surface than is NO. As a result, significant O_3 is produced above 3 km and the maximum O_3 difference appears between 9 and 14 km during the early afternoon hours (from 13:30 to 17:30). However, from surface to about 2 km, O_3 is reduced consistently across the entire period, and this is the result of O_3 titration by NO from cloud-to-ground lightning flashes that must have been transported to this layer by storm downdrafts. Since O_3 is significantly underestimated above 3 km and overestimated near the surface by the Base model, the inclusion of LNO greatly improved the model's performance under both conditions.

Comparison of Figure 9 (mNLDN) with Figure 8 (hNLDN) reveals that the time-sections of NO and NO_x are similar above 5 km but dramatically different near the surface. The near-

surface increase in ambient NO noted in the hNLDN is absent in mNLDN, and in fact there are some small decreases in NO, although the reason for this is unclear. The increase in O_3 aloft in the mNLDN case is similar to that seen in the hNLDN case. However, the near-surface reduction in O_3 is almost absent. In the pNLDN case (Figure 10), NO mixing ratios are much less than those in hNLDN and mNLDN in the upper layers as a result of less column NO being generated by the linear parameterization. The resulting NO_x time-section is also smoothed. The pNLDN time-sections for NO, NO_x and O_3 near the surface are similar to the mNLDN case with no change or small decreases compared to the Base case. O_3 mixing ratios increase by more than 30 ppb during the afternoon hours between 10 – 13 km in the pNLDN case, however the increase is not as intense and widespread as the other cases. In summary, the hNLDN scheme produces estimates that are more consistent with measurements at the surface and aloft, compared to the other simulations, reflecting the advantage of using the spatially and temporally-resolved observed lightning flash data. The model performance improvement for simulated O_3 distributions also suggests robustness in the vertical distribution scheme when LNO is generated at the right time and location.

To corroborate the above time-section distributions of NO, NO_x, and O_3 in the lightning cases, the lightning NO emissions are traced back on July 28 for each case. It is found that in all cases, the lightning NO was injected approximately 200 km upwind (north-west) of the flight path. The hNLDN case captured two injections: one occurred during the morning hours (5:00 to 7:00 am) and the other happened during the afternoon hours (after 2:30 pm). Both mNLDN and pNLND captured the afternoon lightning event at the later time (after 3:30 pm for mNLDN and after 4:30 pm for pNLDN) with varying intensity, but neither captured the morning lightning event, which explains why the increase of NO and NO_x in the hNLDN case (Figure 8) did not occur in the mNLDN and pNLDN cases (Figures 9 and 10). Also note that the significant increase of NO during the time period from 11:00 to 13:00 occurred about 5 hours after the lightning NO was injected at about 200 km upwind in the hNLDN case.

To expand on the evaluation in Figures 7-10 which focused on measurements from July 28, 2011, we retrieved all the P-3B measurements on days with noticeable lightning impact (July 21, 22, 28, and 29). The 3-D paired observation-model data were grouped together by spiral site and the mean biases (model – observation) were plotted in Figure 11 (a and b) for O_3 and NO,

respectively. The boxplots for O_3 in Figure 11a suggests that the Base exhibited larger bias with greater spread (i.e. larger interquartile range) than other model cases incorporating LNO at most of the locations where aircraft spirals were conducted. At all locations except Aldino, the lowest mean biases in simulated NO and O_3 are noted in the hNLDN simulation.

3.3 Deposition evaluation for nitrate

In addition to contributing to tropospheric O_3 formation, NO_x oxidation also leads to gaseous nitric acid and particulate-nitrate which are eventually removed from the atmosphere by dry and wet deposition of nitrate (NO_3^-). As a result, inclusion of NO_x from lightning also plays an important role in nitrogen deposition modeling. To assess the impacts of incorporating LNO emissions on simulated oxidized nitrogen deposition, we compared model estimated amounts of precipitation from NTN network (http://nadp.slh.wisc.edu/ntn/) and wet deposition of NO_3^- with measurements from the NADP network (http://nadp.slh.wisc.edu/). During summer months in 2011 (June -August) the WRF model generally reproduces the observed precipitation with a slight underestimate in the east, but the Base model simulation tends to underestimate wet deposition of NO_3^- across the domain, with the greatest underestimation in the SE and UM (See Table 3 and Figure 12). All three LNO simulations increase wet deposition amounts of NO_3^- and decrease model bias in all regions. The bottom panel of Figure 12 shows that the mNLDN simulation resulted in the largest increase over the base model estimates. The NMB is reduced from -35 % in the Base to -15 % in mNLDN across the domain and from -32 % to -2 % in the SE. The hNLDN shows very similar model performance to the mNLDN case. In contrast, the wet deposition NO_3^- estimates from the pNLDN case are only slightly higher than the Base case, and as a result the evaluation statistics for pNLND are very similar to the Base statistics. As discussed earlier, the mNLDN tends to produce the most LNO among the three LNO schemes, thus it results in the smallest errors in terms of wet deposition of NO_3^- when compared to the Base simulation that significantly underestimated NO_3^- wet deposition. It should be noted that in addition to the LNO contributions, errors in modeled precipitation amounts and patterns also likely influence the underestimation of NO_3^- wet deposition.

4. Conclusions

A detailed evaluation of lightning NO_x emission estimation parameterizations available in the CMAQ modeling system was performed through comparisons of model simulation results with surface and aloft air quality measurements.

Our analysis indicates that incorporation of LNO emissions enhanced O_3 production in the middle and upper troposphere, where O_3 mixing ratios were often significantly underestimated without the representation of LNO. Though the impact on surface O_3 varies from region to region and is also dependent on the accuracy of the NO_x emissions from other sources, the inclusion of LNO, when it is injected at the appropriate time and location, can improve the model estimates. In regions where the base model estimates of O_3 were biased high, the inclusion of LNO further increased the model bias; and a systematic increase is noted in the correlation with measurements, suggesting that emissions from other sources likely drive the overestimation. Identifying how errors in emissions inputs from different sources interact with errors in meteorological modeling of mixing and transport, remains a challenging but critical task. Likewise, all the LNO schemes also enhanced the accumulated wet deposition of NO_3^-, that was significantly underestimated by the base model without LNO throughout the modeling domain except the Pacific Coast.

Uncertainty remains in modeling the magnitude and spatial, temporal and vertical distribution of lightning produced NO_x. LNO schemes are built on numerous assumptions and all current schemes also depend on the skill of the upstream meteorological models in describing convective activity. Nevertheless, these schemes reflect our best understanding and knowledge at the time when the schemes were implemented. The use of hourly information on lightning activity yielded LNO emissions that generally improved model performance for ambient O_3 and NO_x as well as oxidized nitrogen wet deposition amounts. As more high-quality data from both ground and satellite measurements become available, the performance of the LNO schemes will continue to improve.

Since the pNLDN scheme was developed using historical data corelating lightning activity with convective precipitation, the scheme could be employed for applications

involving air quality forecasting and future projections when observed lightning information is not available.

Code and data availability

CMAQ model documentation and released versions of the source code, including all model code used in his study, are available at https://github.com/USEPA/CMAQ/tree/5.2 . The data processing and analysis scripts are available upon request. The WRF model is available for download through the WRF website (http://www2.mmm.ucar.edu/wrf/users/wrfv3.8/updates-3.8.html). The raw lightning flash observation data used are not available to the public but can be purchased through Vaisala Inc. (https:// www.vaisala.com/en/products/systems/lightning-detection). The lightning data obtained from Vaisala Inc. is the cloud-to-ground lightning flashes over the contiguous United States. The immediate data behind the tables and figures are available from https://zenodo.org/record/3360744 (Kang and Foley, 2019). Additional input/output data for CMAQ model utilized for this analysis are available upon request as well.

Disclaimer: The views expressed in this paper are those of the authors and do not necessarily represent the views or policies of the U.S. EPA.

Author Contribution

Daiwen Kang: data collection, algorithm design, model simulation, analysis, and manuscript writing.

Kristen Foley: data analysis and manuscript writing.

Rohit Mathur: manuscript editing.

Shawn Roselle: manuscript editing.

Kenneth Pickering: manuscript editing.

Dale Allen: manuscript editing.

Acknowledgement:

The authors thank Brian Eder, Golam Sarwar, and Janet Burke (U.S. /EPA) for their constructive comments and suggestions during the internal review process.

References

Allen, D., Pickering, K., Stenchikov, G., Thompson, A., and Kondo, Y.: A three-dimensional total odd nitrogen (NOy) simulation during SONEX using a stretched-grid chemical transport model, J. Geophys. Res., 105, 3851–3876, doi:10.1029/1999JD901029, 2000.

Allen, D. J. and Pickering, K. E.: Evaluation of lightning flash rate parameterizations for use in a global chemical transport model, J. Geophys. Res., 107, 4711, doi:10.1029/2002JD002066, 2002.

Allen, D. J., Pickering, K. E., Pinder, R. W., Henderson, B. H., Appel, K. W., and Prados, A.: Impact of lightning-NO on eastern United States photochemistry during the summer of 2006 as determined using the CMAQ model, Atmos. Chem. Phys., 12, 1737–1758, doi:10.5194/acp-12-1737-2012, 2012.

Anderson, D. C., Loughner, C. P., Diskin, G., Weinheimer, A., Canty, T. P., Salawitch, R. J, Worden, H. M., Fried, A., Mikoviny, T., Wisthaler, A., and Dickerson, R. R.: Measured and modeled CO and NOy in DISCOVER-AQ: An evaluation of emissions and chemistry over the eastern US, Atmos. Environ., 96, 78-87, doi:10.1016/j.atmosenv.2014.07.004, 2014.

Appel, K. W., Napelenok, S. L., Foley, K. M., Pye, H. O., Hogrefe, C., Luecken, D. J., Bash, J. O., Roselle, S. J., Pleim, J. E., Foroutan, H., Hutzell1, W. D., Pouliot, G. O., Sarwar, G., Fahey, K. M., Gantt, G., Gilliam, R. C., Heath, N. K., Kang, D., Mathur, R., Schwede, D. B., Spero, T. L., Wong, D. C., and Young, J. O.: Description and evaluation of the Community Multiscale Air Quality (CMAQ) modeling system version 5.1, Geosci. Model Dev., 10, 1703–1732, doi:10.5194/gmd-10-1703-2017, 2017.

Appel, K. W., Foley, K. M., Bash, J. O., Pinder, R. W., Dennis, R. L., Allen, D. J., and Pickering, K.: A multi-resolution assessment of the Community Multiscale Air Quality (CMAQ) model v4.7 wet deposition estimates for 2002-2006, Geosci. Model Dev., 4, 357–371, doi:10.5194/gmd-4-357-2011, 2011.

Bash, J. O., Baker, K. R., and Beaver, M. R.: Evaluation of improved land use and canopy representation in BEIS v3.61 with biogenic VOC measurements in California, Geosci. Model Dev., 9, 2191–2207, doi:10.5194/gmd-9-2191-2016, 2016.

Bovensmann, H., Burrows, J. P., Buchwitz, M., Frerick, J., No¨el, S., Rozanov, V. V., Chance, K. V., and Goede, A. P. H.: SCIAMACHY: Mission Objectives and Measurement Modes, J. Atmos. Sci., 56, 127–150, 1999.c

Brown-Steiner, B., Hess, P. G., and Lin, M. Y.: On the capabilities and limitations of GCCM simulations of summertime regional air quality: A diagnostic analysis of ozone and temperature simulations in the US using CESM CAM-Chem, Atmos. Environ., 101, 134–148, doi:10.1016/j.atmosenv.2014.11.001, 2015

508 Byun, D. W. and Schere, K. L.: Rewiew of the governing equations, computational algorithms,
509 and other components of the Models-3 Community Multiscale Air Quality (CMAQ)
510 modeling system, Appl. Mech. Rev., 59, 51-77, 2006.

511 Canty, T. P., Hembeck, L., Vinciguerra, T. P., Anderson, D. C., Goldberg, D. L., Carpenter, S.
512 F., Allen, D. J., Loughner, C. P., Salawitch, R. J., and Dickerson, R. R.: Ozone and NO_x
513 chemistry in the eastern US: evaluation of CMAQ/CB05 with satellite (OMI) data,
514 Atmos. Chem. Phys., 15, 10965–10982, doi:10.5194/acp-15-10965-2015, 2015.

515 Choi, Y., Wang, Y., Zeng, T., Martin, R. V., Kurosu, T. P., and Chance, K.: Evidence of
516 lightning NO_x and convective transport of pollutants in satellite observations over North
517 America, Geophys. Res. Lett., 32, L02805, doi:10.1029/2004GL021436, 2005.

518 Crawford, J. H. and Pickering, K. E.: DISCOVER-AQ: Advancing strategies for air quality
519 observations for the next decade, EM, A&WMA, September, 2014.

520 Eder, B. K., Kang, D., Mathur, R., Yu, S., and Schere, K.: An operational evaluation of the Eta-
521 CMAQ air quality forecast model, Atmos. Environ., 40, 4894-4905, 2006.

522 Finney, D. L., Doherty, R. M., Wild, O., Huntrieser, H., Pumphrey, H. C., and Blyth, A. M.:
523 Using cloud ice flux to parametrize large-scale lightning, Atmos. Chem. Phys., 14,
524 12665–12682, doi:10.5194/acp-14-12665-2014, 2014.

525 Finney, D. L., Doherty, R. M., Wild, O., and Abraham, N. L.: The impact of lightning on
526 tropospheric ozone chemistry using a new global lightning parameterization, Atmos.
527 Chem. Phys., 16, 7507–7522, doi:10.5194/acp-16-7507-2016, 2016.

528 Fiore, A. M., Dentener, F. J., Wild, O., Cuvelier, C., Schultz, M. G., Hess, P., Textor, C., Schulz,
529 M., Doherty, R. M., Horowitz, L. W., MacKenzie, I. A., Sanderson, M. G., Shindell, D.
530 T., Stevenson, D. S., Szopa, S., Van Dingenen, R., Zeng, G., Atherton, C., Bergmann, D.,
531 Bey, I., Carmichael, G., Collins, W. J., Duncan, B. N., Faluvegi, G., Folberth, G., Gauss,
532 M., Gong, S., Hauglustaine, D., Holloway, T., Isaksen, I. S. A., Jacob, D. J., Jonson, J. E.,
533 Kaminski, J. W., Keating, T. J., Lupu, A., Marmer, E., Montanaro, V., Park, R. J., Pitari,
534 G., Pringle, K. J., Pyle, J. A., Schroeder, S., Vivanco, M. G., Wind, P., Wojcik, G., Wu,
535 S., and Zuber, A.: Multimodel estimates of intercontinental sourcereceptor relationships
536 for ozone pollution, J. Geophys. Res., 114, D04301, doi:10.1029/2008jd010816, 2009.

537 Foley, K. M., Roselle, S. J., Appel, K. W., Bhave, P. V., Pleim, J. E., Otte, T. L., Mathur, R.,
538 Sarwar, G., Young, J. O., Gilliam, R. C., Nolte, C. G., Kelly, J. T., Gilliland, A. B., and
539 Bash, J. O.: Incremental testing of the Community Multiscale Air Quality (CMAQ)
540 modeling system version 4.7, Geosci. Model Dev., 3, 205–226, doi:10.5194/gmd-3-205-
541 2010, 2010.

542 Follette-Cook, M. B., Pickering, K. E., Crawford, J. H., Duncan, B. N., Loughner, C. P., Diskin,
543 G. S., Fried, A., and Weinheimer, A. J.: Spatial and temporal variability of trance gas
544 columns derived from WRF/Chem regional model output: Planning for geostationary

observations of atmospheric composition, Atmos. Environ., 118, 28-44, doi:10.1016/j.atmosenv.2015.07.024, 2015.

Kang, D., Eder, B. K., Stein, A. F., Grell, G. A., Peckham, S. E., and Mchenry, J.: The New England air quality forecasting pilot program: development of an evaluation protocol and performance benchmark, J. Air & Waste Manage. Assoc., 55, 1782-1796, 2005.

Kang, D., and Foley, K.**:** Simulating Lightning NO Production in CMAQv5.2: Performance Evauations, data set, https://doi.org/10.5281/zenodo.3360744 , 2019.

Kang, D., Pickering, K. E., Allen, D. J., Foley, K. M., Wong, D., Mathur, R., and Roselle, S. J.: Simulating Lightning NO Production in CMAQv5.2: Evolution of Scientific Updates, Geosci. Model Dev., 12, 3071–3083, doi:10.5194/gmd-12-3071-2019, 2019.

Kang, D. and Pickering, K. E.: Lightning NO_x emissions and the Implications for Surface Air Quality over the Contiguous United States, EM, A&WMA, November, 2018.

Kaynak, B., Hu, Y., Martin, R. V., Russell, A. G., Choi, Y., and Wang, Y.: The effect of lightning NO*x* production on surface ozone in the continental United States. Atmos Chem Phys. 8(17):5151–5159. doi:10.5194/acp-8-5151-2008, 2008.

Koo, B., Chien, C. J., Tonnesen, G., Morris, R., Johnson, J., Sakulyanontvittaya T., Piyachaturawat, P., and Yarwood, G.: Natural emissions for regional modeling of background ozone and particulate matter and impacts on emissions control strategies. Atmos Environ.,44(19):2372–2382. doi:10.1016/j.atmosenv.2010.02.041, 2010.

Koshak, W., Peterson, H., Biazar, A., Khan, M., and Wang, L.: The NASA Lightning Nitrogen Oxides Model (LNOM): Application to air quality modeling, Atmos. Res., doi:10.1016/j.atmosres.2012.12.015, 2014.

Labrador, L. J., von Kuhlmann, R., and Lawrence, M. G.: The effects of lightning-produced NO_x and its vertical distribution on atmospheric chemistry: sensitivity simulations with MATCHMPIC, Atmos. Chem. Phys., 5, 1815–1834, 2005,

Lin, J., Youn, D., Liang, X., and Wuebbles, D.: Global model simulation of summertime U.S. ozone diurnal cycle and its sensitivity to PBL mixing, spatial resolution, and emissions, Atmos. Environ., 42, 8470–8483, doi:10.1016/j.atmosenv.2008.08.012, 2008.

Murray, L. T.: Lightning NO_x and Impacts on Air Quality, *Curr Pollution Rep.,* doi: 10.1007/s40726-016-0031-7, 2016.

Nolte, C. G., Appel, K. W., Kelly, J. T., Bhave, P. V., Fahey, K. M., Collett Jr., J. L., Zhang, L., and Young, J. O.: Evaluation of the Community Multiscale Air Quality (CMAQ) model v5.0 against size-resolved measurements of inorganic particle composition across sites in North America, Geosci. Model Dev., 8, 2877–2892, doi:10.5194/gmd-8-2877-2015, 2015.

Napelenok, S. L., Pinder, R. W., Gilliland, A. B., and Martin, R. V.: A method for evaluating spatially-resolved NO_x emissions using Kalman filter inversion, direct sensitivities, and spacebased NO_2 observations, Atmos. Chem. Phys., 8, 5603–5614, doi:10.5194/acp-8-5603-2008, 2008.

Novak, J. H. and Pierce, T. E.: Natural emissions of oxidant precursors, Water Air Soil Poll., 67, 57-77, 1993.

Orville, R. E., Huffines, G. R., Burrows, W. R., Holle, R. L., and Cummins, K. L.: The North American Lightning Detection Network (NALDN) – first results: 1998-2000, Mon. Wea. Rev., 130, 2098–2109, 2002.

Otte, T. L. and Pleim, J. E.: The Meteorology-Chemistry Interface Processor (MCIP) for the CMAQ modeling system: updates through MCIPv3.4.1, Geosci. Model Dev., 3, 243–256, doi:10.5194/gmd-3-243-2010, 2010.

Pickering, K. E., Bucsela, E., Allen, D., Ring, A., Holzworth, R., and Krotkov, N.: Estimates of lightning NO_x production based on OMI NO2 observations over the Gulf of Mexico, J. Geophys. Res. Atmos., 121, 8668–8691, doi:10.1002/2015JD024179, 2016.

Price, C., Penner, J., and Prather, M.: NO_x from lightning. 2. Constraints from the global atmospheric electric circuit, J. Geophys. Res., 102, 5943–5951, doi:10.1029/96JD02551, 1997.

Price, C. and Rind, D.: A simple lightning parameterization for calculating global lightning distributions, J. Geophys. Res., 97, 9919–9933, doi:10.1029/92JD00719, 1992.

Richter, A., Burrows, J. P., N¨uß, H., Granier, C., and Niemeier, U.: Increase in tropospheric nitrogen dioxide over China observed from space, Nature, 437, 129–132, doi:10.1038/nature04092, 2005.

Rossow, W. B., Walker, A. W., Beuschel, D. E., and Roiter, M. D.: International Satellite Cloud Climatology Project (ISCCP) documentation of new cloud data sets, Tech. Rep. January, World Meteorological Organisation, WMO/TD 737, Geneva, 1996.

Schumann, U. and Huntrieser, H.: The global lightning-induced nitrogen oxides source, Atmos. Chem. Phys., 7, 3823-3907, doi:10.5194/acp-7-3823-2007, 2007.

Sioris, C. E., Kurosu, T. P., Martin, R. V., and Chance, K.: Stratospheric and tropospheric NO2 observed by SCIAMACHY: first results, Adv. Space Res., 34, 780–785, 2004.

Stockwell, D. Z., Giannakopoulos, C., Plantevin, P. H., Carver, G. D., Chipperfield, M. P., Law, K. S., Pyle, J. A., Shallcross, D. E., and Wang, K. Y.: Modelling NO_x from lightning and its impact on global chemical fields, Atmos. Environ., 33, 4477–4493, 1999.

Smith, S. N., and Mueller, S. F.: Modeling natural emissions in the Community Multiscale Air Quality (CMAQ) Model-I: building an emissions data base. Atmos Chem Phys., 10(10):4931–4952. doi:10.5194/acp-10-4931-2010, 2010.

Simon, H., Reff, A., Wells, B., Xing, J., and Frank, N.: Ozone trends across the United States over a period of decreasing NO_x and VOC emissions. Environ. Sci. Technol., 49, 186-195, 2015.

Wang, L., Newchurch, M. J., Pour-Biazar, A., Kuang, S., Khan, M., Liu, X., Koshak, W., and Chance, K.: Estimating the influence of lightning on upper tropospheric ozone using NLDN lightning data and CMAQ model, Atmos. Environ., 67, 219–228, 2013.

Yarwood, G., Whitten, G. Z., Jung, J., Heo, G., and Allen, D. T.: Final Report: Development, Evaluation and Testing of Version 6 of the Carbon Bond Chemical Mechanism (CB6), available at: https://www.tceq.texas.gov/assets/public/implementation/air/am/contracts/reports/pm/5820784005FY1026-20100922-environ-cb6.pdf, 2010.

Figure Captions:

Figure 1. Analysis regions and ozonesonde locations during the 2011 DISCOVER-AQ field study.

Figure 2. Timeseries of regional-mean daily maximum 8-hr O_3 comparing observations (AQS) and CMAQ model predictions using the LNO_x schemes to Base simulation for the domain (a), SE (b), and RM (c) in July 2011. The numbers in the parentheses following the region names are the number of AQS sites.

Figure 3. Timeseries of daily mean NO_X over the domain (a), SE (b), and RM (c) in July 2011. The numbers in the parentheses following the region names are the number of AQS sites.

Figure 4. Diurnal profiles for hourly O_3 and NO_x over the domain (a,d), SE (b,e), and RM (c,f) in July 2011.

Figure 5. Spatial maps of the mean bias of DM8HR O_3 (model – observation) differences between model case with LNO_X and the Base as well as the corresponding histograms indicating the number of sites with decreased mean bias for each pair of model cases in July 2011.

Figure 6. Vertical profiles of O_3 mixing ratios from ozonesonde measurements and model simulations at Beltsville, MD (a) and Edgewood, MD (b) on the days when lightning NO produced significant impact on O_3 during the Discover-AQ field study in July 2011.

Figure 7. Overlay of P3B observed O_3 (1-minute mean values) over the corresponding vertical cross sections of simulated values extracted at the flying locations on July 28, 2018, (a) Base, (b) hNLDN (c) mNLDN, and (d) pNLDN. The letters marked at the bottom of the plots are P3B spiral sites, Be: Beltsville, Pa: Padonia, Fa: Fairhill, Al: Aldino, Ed: Edgewood, Es: Essex.

Figure 8. The vertical-time difference between hNLDN and Base during the P3B flight period on July 28, 2011 for (a) NO, (b) NO_X, and (c) O_3.

713 Figure 9. The vertical-time difference between mNLDN and Base during the P3B flight period
714 on July 28, 2011 for (a) NO, (b) NO_X, and (c) O_3.

715 Figure 10. The vertical-time difference between pNLDN and Base during the P3B flight period
716 on July 28, 2011 for (a) NO, (b) NO_X, and (c) O_3.

717 Figure 11. Bias (model – observation) distributions of O_3 (a) and NO (b) at each P3B spiral site
718 on July 21, 22, 28, and 29, 2011. Be: Beltsville, Pa: Padonia, Fa: Fairhill, Al: Aldino, Ed:
719 Edgewood, Es: Essex, Cb: Chesapeake Bay

720 Figure 12. The top row shows precipitation estimates from WRF (left), the bias in the WRF
721 predicted precipitation at NTN locations (middle), and the corresponding scatter plots
722 (right). The middle row shows wet deposition (Dep) of nitrate estimates from the Base
723 simulation (left), the bias in the Base model estimates of wet deposition of NO_3^- at
724 NADP/NTN locations (middle), and the corresponding scatter plots (right). The bottom
725 row shows the difference in the LNO_X sensitivity simulations and the Base case estimates
726 of wet deposition of NO_3^-: mNLDN – Base (left); hNLDN – Base (middle), and pNLDN
727 – Base (right). All maps are based on accumulated values (precipitation or wet
728 deposition) during June – August 2011. Precipitation totals are in cm and wet deposition
729 totals are in kg/ha.

Figure Captions:

Figure 1. Analysis regions and ozonesonde locations during the 2011 DISCOVER-AQ field study.

Figure 2. Timeseries of regional-mean daily maximum 8-hr O_3 comparing observations (AQS) and CMAQ model predictions using the LNO_x schemes to Base simulation for the domain (a), SE (b), and RM (c) in July 2011. The numbers in the parentheses following the region names are the number of AQS sites.

Figure 3. Timeseries of daily mean NO_X over the domain (a), SE (b), and RM (c) in July 2011. The numbers in the parentheses following the region names are the number of AQS sites.

Figure 4. Diurnal profiles for hourly O_3 and NO_x over the domain (a,d), SE (b,e), and RM (c,f) in July 2011.

Figure 5. Spatial maps of the mean bias of DM8HR O_3 (model – observation) differences between model case with LNO_X and the Base as well as the corresponding histograms indicating the number of sites with decreased mean bias for each pair of model cases in July 2011.

Figure 6. Vertical profiles of O_3 mixing ratios from ozonesonde measurements and model simulations at Beltsville, MD (a) and Edgewood, MD (b) on the days when lightning NO produced significant impact on O_3 during the Discover-AQ field study in July 2011.

Figure 7. Overlay of P3B observed O_3 (1-minute mean values) over the corresponding vertical cross sections of simulated values extracted at the flying locations on July 28, 2018, (a) Base, (b) hNLDN (c) mNLDN, and (d) pNLDN. The letters marked at the bottom of the plots are P3B spiral sites, Be: Beltsville, Pa: Padonia, Fa: Fairhill, Al: Aldino, Ed: Edgewood, Es: Essex.

Figure 8. The vertical-time difference between hNLDN and Base during the P3B flight period on July 28, 2011 for (a) NO, (b) NO_X, and (c) O_3.

Figure 9. The vertical-time difference between mNLDN and Base during the P3B flight period on July 28, 2011 for (a) NO, (b) NO_X, and (c) O_3.

Figure 10. The vertical-time difference between pNLDN and Base during the P3B flight period on July 28, 2011 for (a) NO, (b) NO_X, and (c) O_3.

Figure 11. Bias (model – observation) distributions of O_3 (a) and NO (b) at each P3B spiral site on July 21, 22, 28, and 29, 2011. Be: Beltsville, Pa: Padonia, Fa: Fairhill, Al: Aldino, Ed: Edgewood, Es: Essex, Cb: Chesapeake Bay

Figure 12. The top row shows precipitation estimates from WRF (left), the bias in the WRF predicted precipitation at NTN locations (middle), and the corresponding scatter plots (right). The middle row shows wet deposition (Dep) of nitrate estimates from the Base simulation (left), the bias in the Base model estimates of wet deposition of NO_3^- at NADP/NTN locations (middle), and the corresponding scatter plots (right). The bottom row shows the difference in the LNO_X sensitivity simulations and the Base case estimates of wet deposition of NO_3^-: mNLDN – Base (left); hNLDN – Base (middle), and pNLDN – Base (right). All maps are based on accumulated values (precipitation or wet deposition) during June – August 2011. Precipitation totals are in cm and wet deposition totals are in kg/ha.

Table 1. Statistics of DM8HR O_3 for all model cases over the domain and analysis regions in July 2011. The best performance metrics among the model cases are highlighted in bold.

Region	Case	Record	OBS (ppb)	MOD (ppb)	RMSE (ppb)	NME (%)	MB (ppb)	NMB (%)	R
Domain	Base	36242	48.21	52.04	12.6	19.2	**3.8**	**8.0**	0.69
	mNLDN	36242	48.21	53.40	12.9	19.8	5.2	10.8	0.70
	hNLDN	36242	48.21	52.21	**11.9**	**18.4**	4.0	8.3	**0.72**
	pNLDN	36242	48.21	52.52	12.7	19.5	4.3	8.9	0.70
NE	Base	5512	50.97	55.08	13.0	17.8	4.1	8.1	0.74
	mNLDN	5512	50.97	55.77	13.4	18.5	4.8	9.4	0.74
	hNLDN	5512	50.97	54.23	**11.9**	**16.7**	**3.3**	**6.4**	**0.75**
	pNLDN	5512	50.97	55.32	13.1	18.0	4.4	8.5	0.74
SE	Base	7061	44.55	51.71	**12.6**	**21.0**	**7.2**	**16.1**	0.76
	mNLDN	7061	44.55	53.33	13.6	236	8.8	19.7	0.76
	hNLDN	7061	44.55	52.30	12.6	21.7	7.8	17.4	**0.77**
	pNLDN	7061	44.55	52.39	13.0	22.0	7.8	17.6	0.76
UM	Base	8072	51.60	58.99	13.6	18.8	7.4	14.3	0.64
	mNLDN	8072	51.60	60.14	14.4	20.5	8.5	16.6	0.64
	hNLDN	8072	51.60	58.35	**12.8**	**18.0**	**6.8**	**13.1**	0.64
	pNLDN	8072	51.60	59.42	13.9	19.4	7.8	15.1	0.64
LM	Base	3609	42.15	46.21	12.4	21.5	**4.1**	**9.6**	0.73
	mNLDN	3609	42.15	47.93	12.9	22.3	5.8	13.7	0.74
	hNLDN	3609	42.15	47.12	**12.3**	**21.3**	5.0	11.8	**0.76**
	pNLDN	3609	42.15	46.93	12.6	21.8	4.8	11.3	0.74
RM	Base	6256	52.52	48.13	11.3	17.0	-4.4	-8.4	0.52
	mNLDN	6256	52.52	50.93	10.2	14.7	**-1.6**	**-3.0**	0.56
	hNLDN	6256	52.52	50.35	**9.9**	**14.4**	-2.2	-4.1	**0.57**
	pNLDN	6256	52.52	48.93	10.9	16.2	-3.6	-6.9	0.53
PC	Base	5570	44.72	47.58	11.7	20.1	2.9	6.4	0.80
	mNLDN	5570	44.72	47.73	11.6	20.0	3.0	6.7	0.80
	hNLDN	5570	44.72	46.65	**11.3**	**19.5**	**1.9**	**4.3**	**0.81**
	pNLDN	5570	44.72	47.62	11.6	20.0	2.9	6.5	0.80

Table 2. Statistics of daily mean NO_X for all model cases over the domain and analysis regions July 2011. The best performance metrics among the model cases are highlighted in bold.

Region	Case	Record	OBS (ppb)	MOD (ppb)	RMSE (ppb)	NME (%)	MB (ppb)	NMB (%)	R
Domain	Base	6912	7.58	8.88	**8.7**	62.6	**1.3**	17.1	0.54
	mNLDN	6912	7.58	8.87	**8.7**	**62.5**	**1.3**	**17.1**	0.54
	hNLDN	6912	7.58	8.92	8.7	62.7	1.3	17.7	**0.55**
	pNLDN	6912	7.58	8.87	**8.7**	62.5	**1.3**	17.1	0.54
NE	Base	989	10.48	9.72	**7.0**	46.0	-0.8	-7.3	0.55
	mNLDN	989	10.48	9.71	**7.0**	**46.0**	-0.8	-7.3	**0.55**
	hNLDN	989	10.48	9.77	7.1	46.1	**-0.7**	**-6.8**	0.55
	pNLDN	989	10.48	9.72	**7.0**	46.0	-0.8	-7.3	0.55
SE	Base	645	6.44	9.18	7.2	75.3	2.7	42.6	0.34
	mNLDN	645	6.44	9.17	**7.2**	**75.1**	**2.7**	**42.4**	0.34
	hNLDN	645	6.44	9.18	7.2	75.3	2.7	42.6	**0.34**
	pNLDN	645	6.44	9.17	7.2	75.2	2.7	42.5	0.34
UM	Base	542	11.42	18.09	**18.7**	**82.7**	**6.7**	**58.4**	**0.58**
	mNLDN	542	11.42	18.10	18.7	82.8	6.7	58.5	**0.58**
	hNLDN	542	11.42	18.22	18.9	83.6	6.8	59.5	**0.58**
	pNLDN	542	11.42	18.09	18.7	**82.7**	**6.7**	58.4	**0.58**
LM	Base	1240	6.11	8.32	6.0	61.2	2.2	36.1	**0.68**
	mNLDN	1240	6.11	8.30	**6.0**	**61.1**	**2.2**	**35.9**	**0.68**
	hNLDN	1240	6.11	8.33	6.0	61.3	2.2	36.3	**0.68**
	pNLDN	1240	6.11	8.31	6.0	61.2	2.2	36.0	**0.68**
RM	Base	1370	3.90	4.00	3.7	60.0	**0.1**	**2.4**	0.58
	mNLDN	1370	3.90	4.01	**3.7**	**59.9**	**0.1**	2.6	0.58
	hNLDN	1370	3.90	4.02	3.7	60.0	0.1	3.3	**0.58**
	pNLDN	1370	3.90	4.00	3.7	60.0	**0.1**	**2.4**	0.58
PC	Base	2056	8.61	9.52	**9.1**	**62.8**	**0.9**	**10.6**	0.48
	mNLDN	2056	8.61	9.52	**9.1**	**62.8**	**0.9**	**10.6**	0.48
	hNLDN	2056	8.61	9.59	9.1	62.9	1.0	11.4	**0.48**
	pNLDN	2056	8.61	9.52	**9.1**	**62.8**	**0.9**	**10.6**	0.48

Table 3. Statistics of June-August 2011 accumulated precipitation (cm) and wet deposition of nitrate (NO_3^-) for all model cases over the domain. The best performance metrics among the model cases are highlighted in bold.

Region	Case	Record	OBS (cm, kg/ha)	MOD (cm, kg/ha)	RMSE (cm, kg/ha)	NME (%)	MB (cm, kg/ha)	NMB (%)	R
Domain	precip	196	24.8	23.9	7.5	23	-0.9	-4	0.87
	Base	196	2.34	1.52	1.1	38	-0.8	-35	0.84
	mNLDN	196	2.34	1.98	**0.8**	**26**	**-0.4**	**-15**	**0.86**
	hNLDN	196	2.34	1.95	**0.8**	**26**	**-0.4**	-17	**0.86**
	pNLDN	196	2.34	1.68	1.0	33	-0.7	-28	0.85
NE	precip	31	38.6	35.9	9.5	19	-2.7	-7	0.79
	Base	31	2.96	2.32	1.1	29	-0.6	-23	0.70
	mNLDN	31	2.96	2.71	**0.9**	**24**	-0.3	-8	**0.76**
	hNLDN	31	2.96	2.74	**0.9**	**24**	**-0.2**	**-7**	0.74
	pNLDN	31	2.96	2.48	1.0	27	-0.5	-16	0.73
SE	precip	39	36.1	31.7	9.4	21	-4.3	-12	0.80
	Base	39	3.05	2.09	1.2	35	-1.0	-32	0.51
	mNLDN	39	3.05	2.97	**0.8**	**21**	**-0.1**	**-2**	**0.56**
	hNLDN	39	3.05	2.82	0.9	23	-0.2	-8	0.53
	pNLDN	39	3.05	2.43	1.0	27	-0.6	-20	0.54
UM	precip	45	28.8	26.1	6.8	20	-2.7	-9	0.51
	Base	45	3.17	1.98	1.4	38	-1.2	-38	0.73
	mNLDN	45	3.17	2.51	**0.9**	**24**	**-0.7**	**-21**	**0.77**
	hNLDN	45	3.17	2.48	**0.9**	25	**-0.7**	-22	**0.77**
	pNLDN	45	3.17	2.15	1.2	33	-1.0	-32	0.76
LM	precip	12	12.3	10.4	4.1	29	-2.0	-16	0.90
	Base	12	1.44	0.85	0.7	41	-0.6	-41	0.90
	mNLDN	12	1.44	1.16	**0.6**	33	**-0.3**	**-19**	0.88
	hNLDN	12	1.44	1.13	**0.6**	**32**	**-0.3**	-21	**0.89**
	pNLDN	12	1.44	0.93	0.7	36	-0.5	-35	0.88
RM	precip	50	13.7	18.2	6.9	39	4.4	32	0.91
	Base	50	1.63	0.8	1.0	51	-0.8	-51	0.90
	mNLDN	50	1.63	1.1	**0.7**	34	**-0.5**	-32	**0.91**
	hNLDN	50	1.63	1.12	**0.7**	**33**	**-0.5**	**-31**	0.90
	pNLDN	50	1.63	0.86	1.0	48	-0.8	-47	**0.91**
PC	precip	19	7.01	6.53	**2.4**	29	**-0.48**	-6.8	0.84
	Base	19	0.31	0.31	**0.18**	44	**0.00**	-1.0	0.88
	mNLDN	19	0.31	0.33	0.19	48	0.01	3.9	**0.89**
	hNLDN	19	0.31	0.33	0.20	50	0.02	6.6	**0.89**
	pNLDN	19	0.31	0.31	**0.18**	44	**0.00**	**-0.3**	0.88

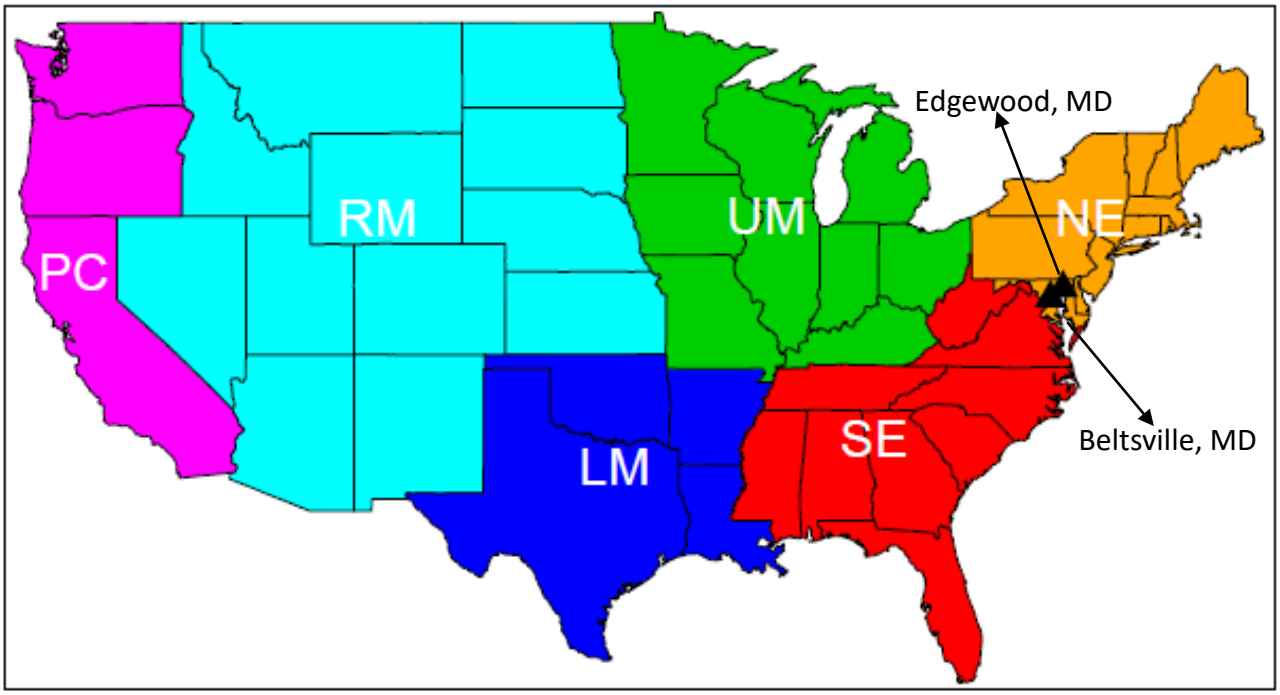

Figure 1. Analysis regions and ozonesonde locations during the 2011 DISCOVER-AQ field study.

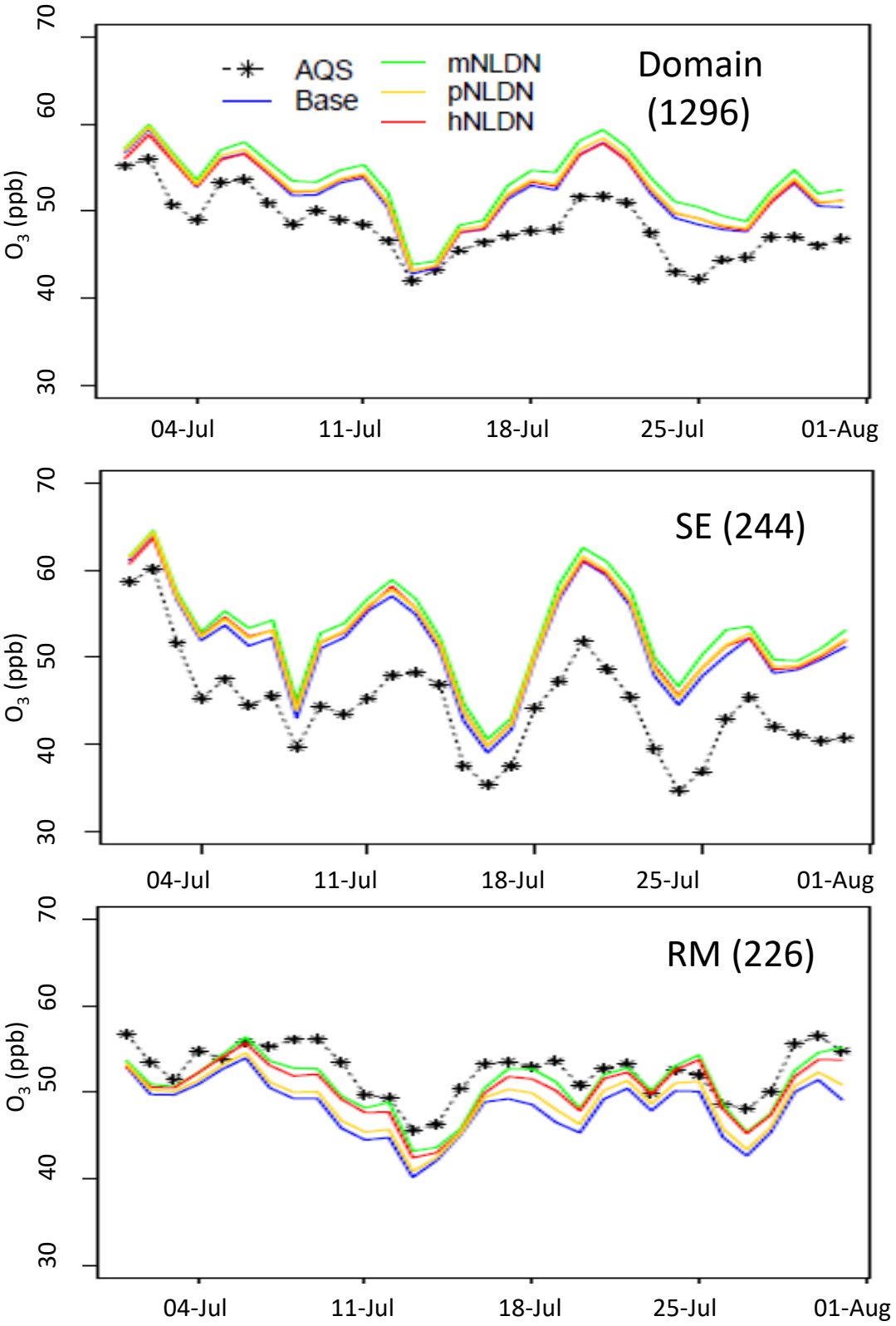

Figure 2. Timeseries of regional-mean daily maximum 8-hr O_3 comparing observations (AQS) and CMAQ model predictions using the LNO_x schemes to Base simulation for the domain (a), SE (b), and RM (c) in July, 2011. The numbers in the parentheses following the region names are the number of AQS sites.

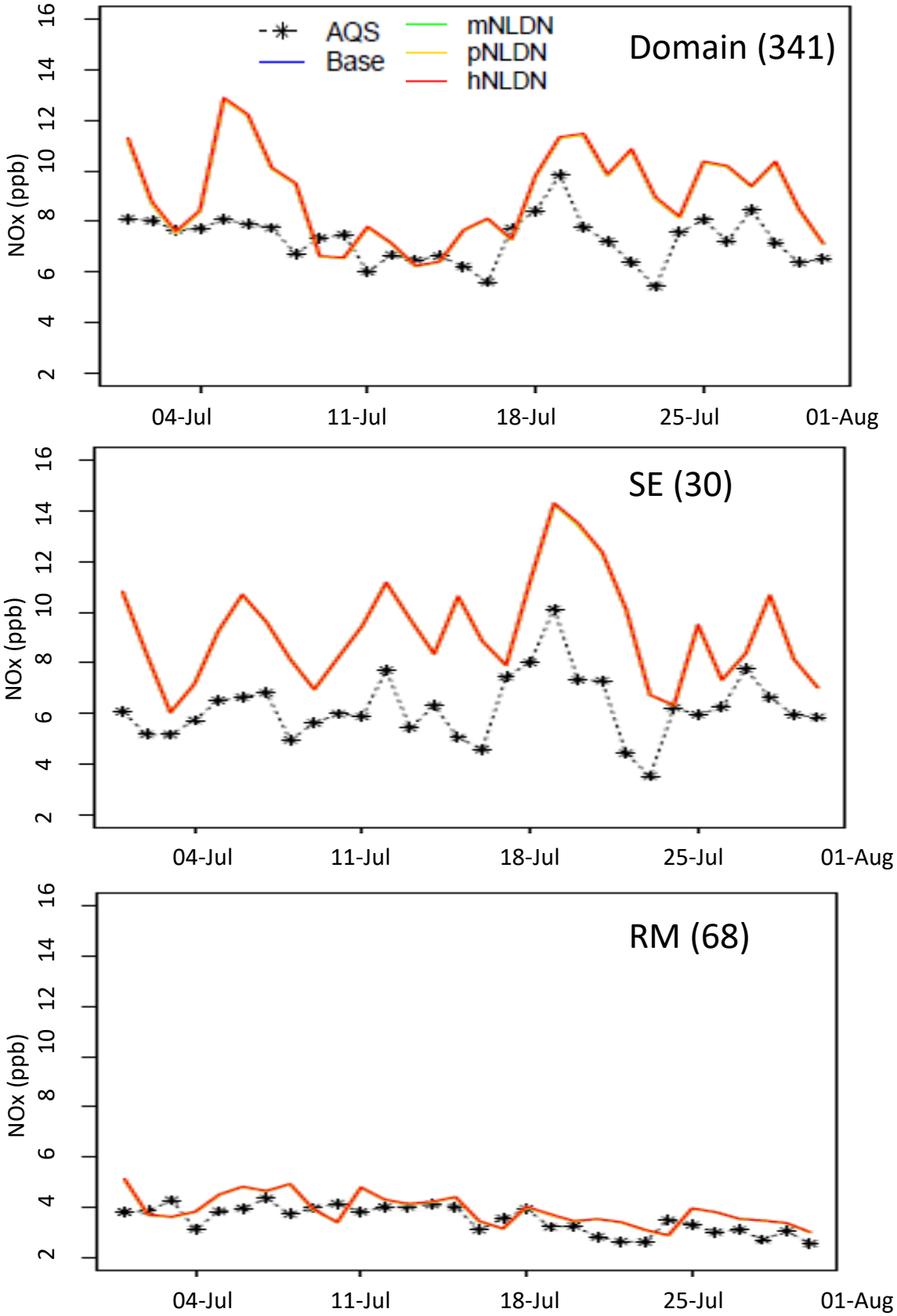

Figure 3. Timeseries of daily mean NO_X over the domain (a), SE (b), and RM (c) in July, 2011. The numbers in the parentheses following the region names are the number of AQS sites.

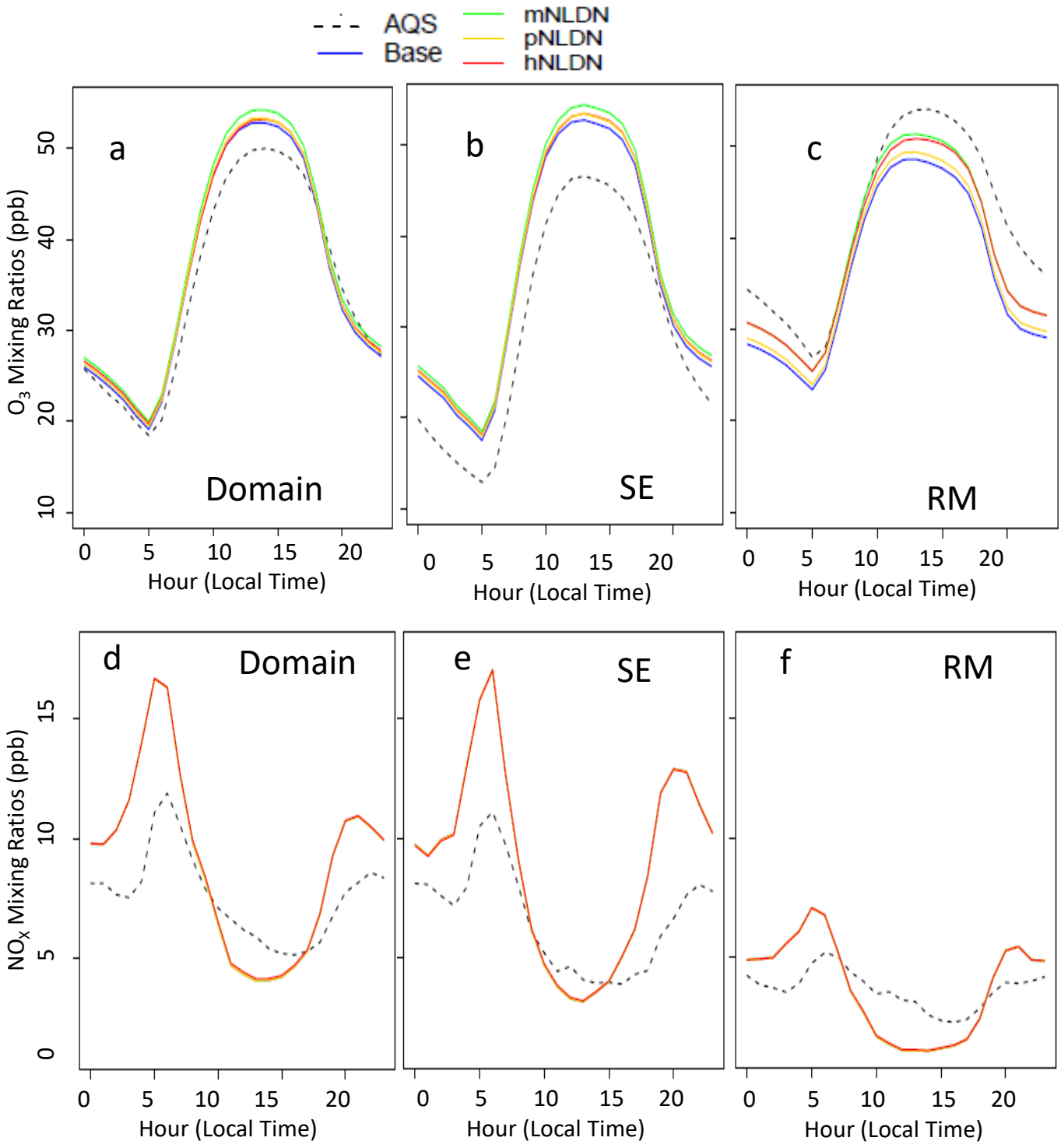

Figure 4. Diurnal profiles for hourly O_3 and NO_X over the domain (a,d), SE (b,e), and RM (c,f) in July, 2011.

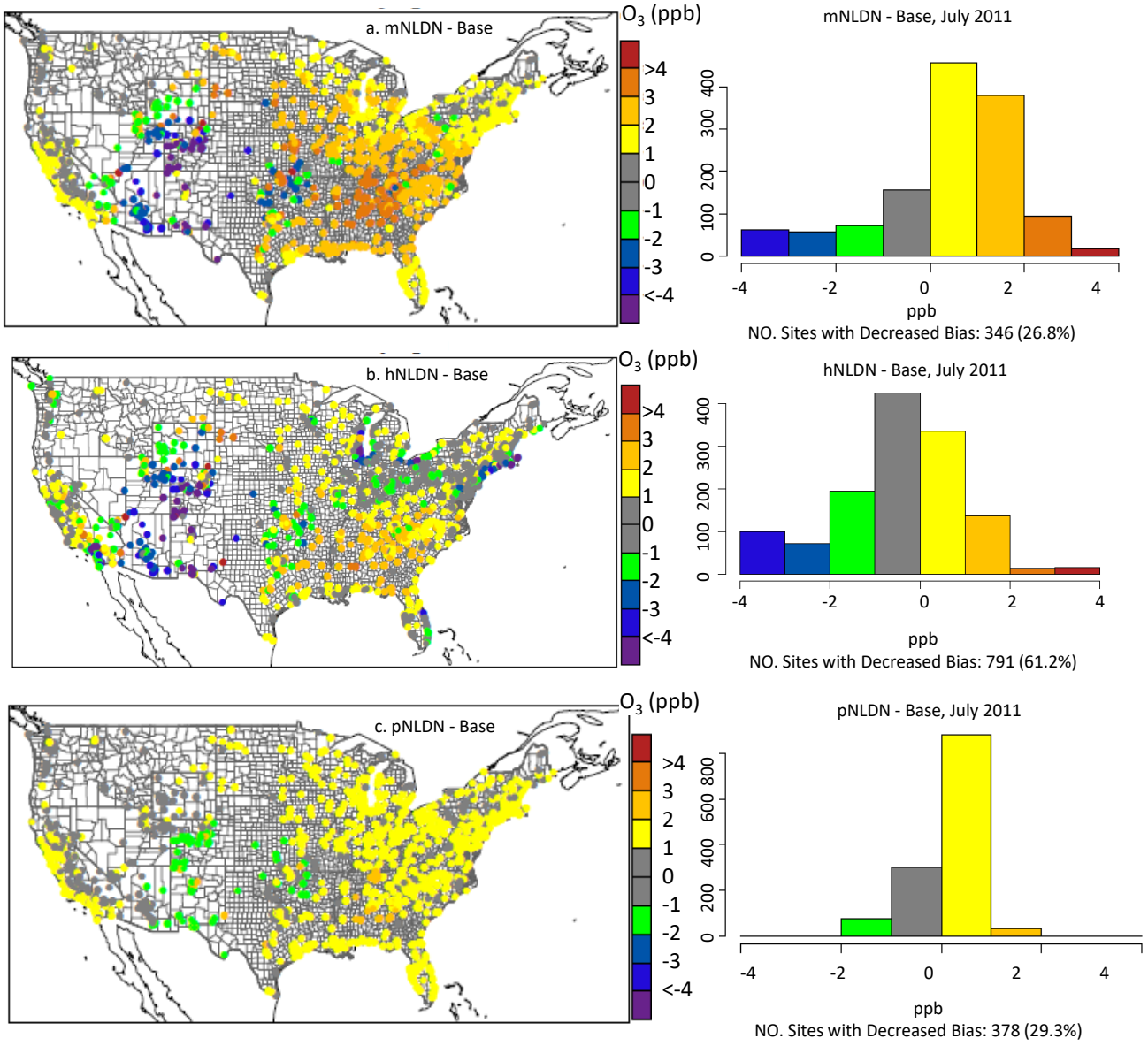

Figure 5. Spatial maps of the mean bias of DM8HR O_3 (model – observation) differences between model case with LNO_X and the Base as well as the corresponding histograms indicating the number of sites with decreased mean bias for each pair of model cases in July, 2011.

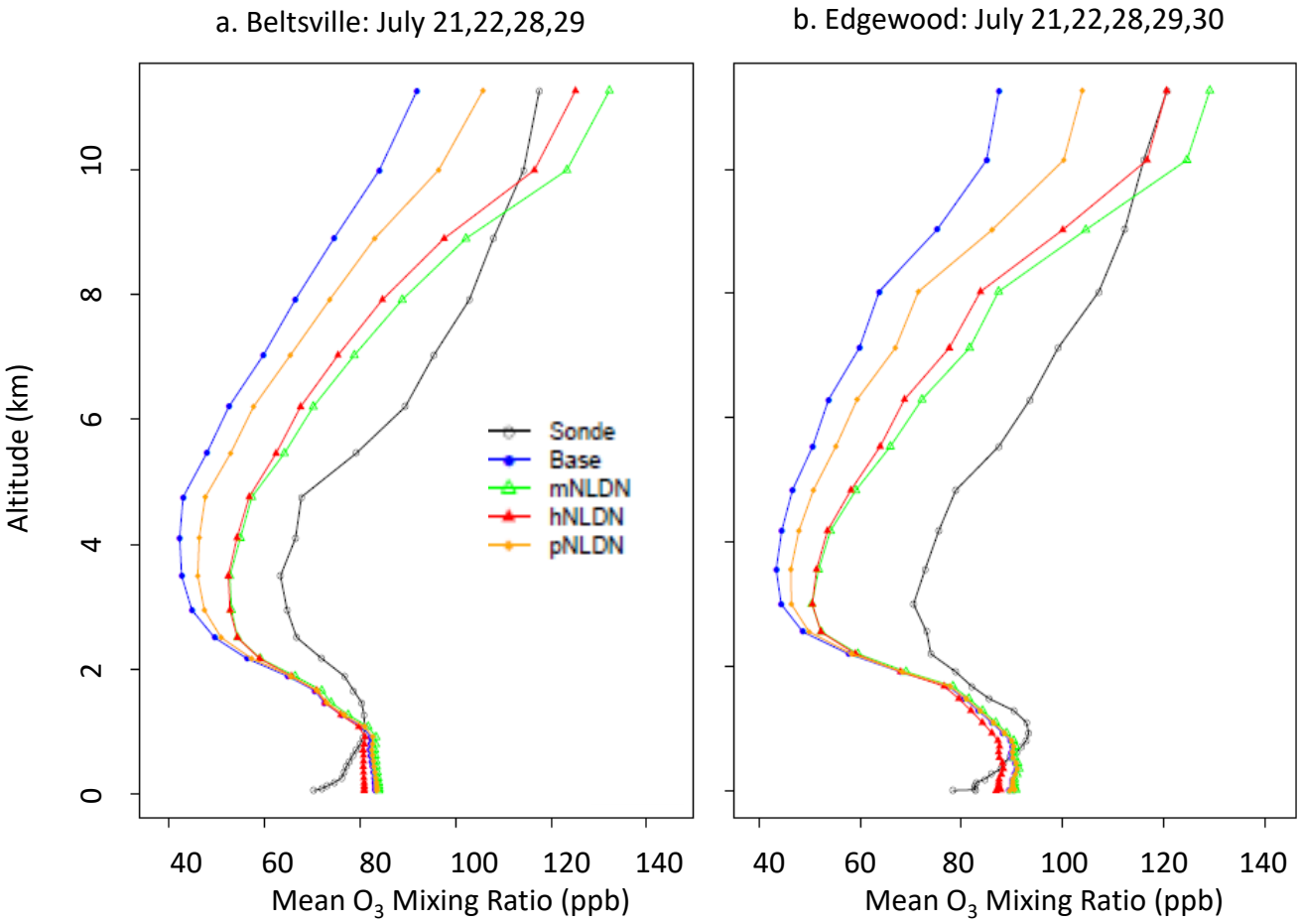

Figure 6. Vertical profiles of O_3 mixing ratios from ozonesonde measurements and model simulations at Beltsville, MD (a) and Edgewood, MD (b) on the days when lightning NO produced significant impact on O_3 during the Discover-AQ field study in July, 2011.

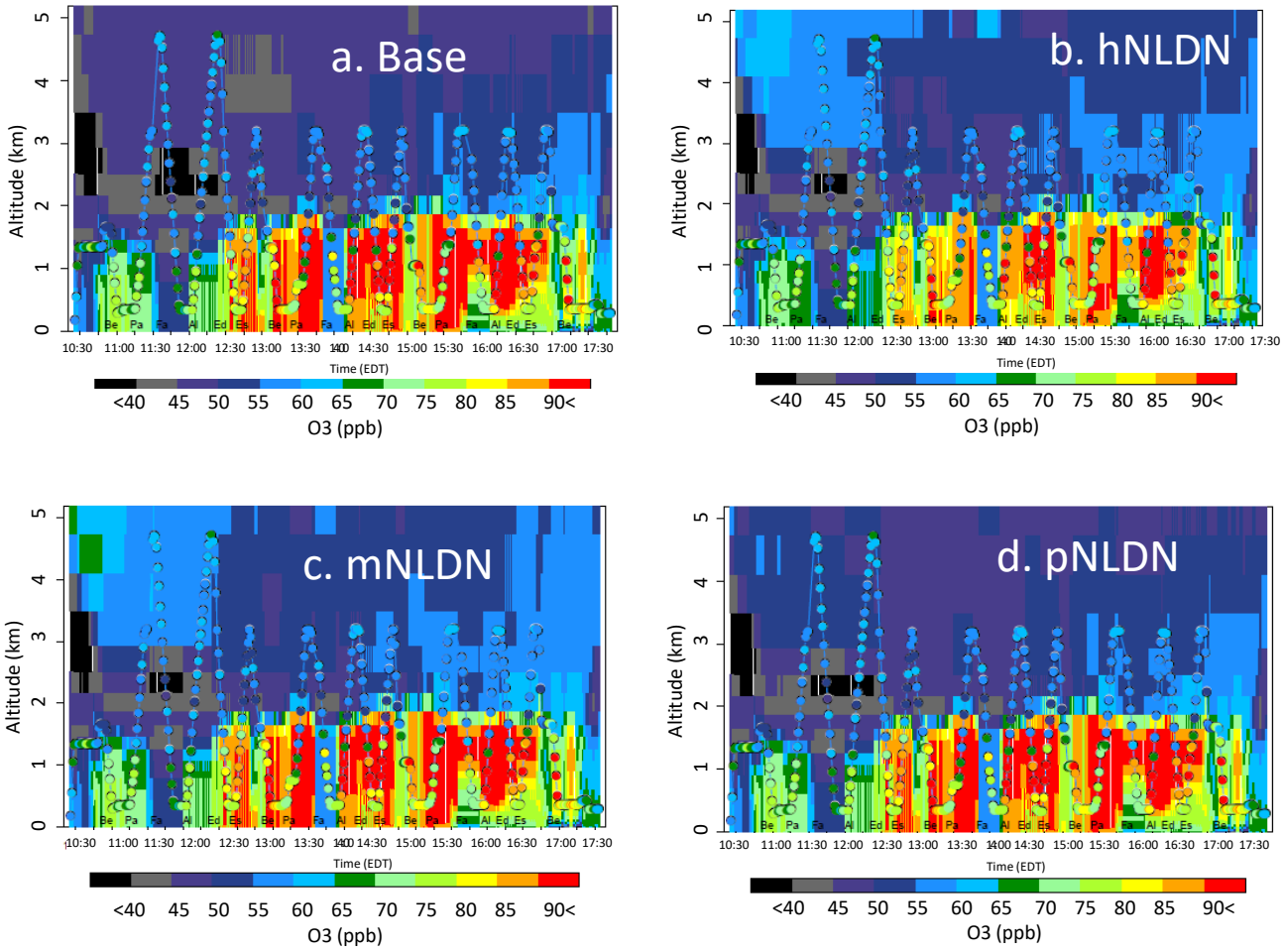

Figure 7. Overlay of P3B observed O_3 (1 minute mean values) over the corresponding vertical cross sections of simulated values extracted at the flying locations on July 28, 2018, (a) Base, (b) hNLDN,(c) mNLDN, and (d) pNLDN. The letters marked at the bottom of the plots are P3B spiral sites, Be: Beltsville, Pa: Padonia, Fa: Fairhill, Al: Aldino, Ed: Edgewood, Es: Essex.

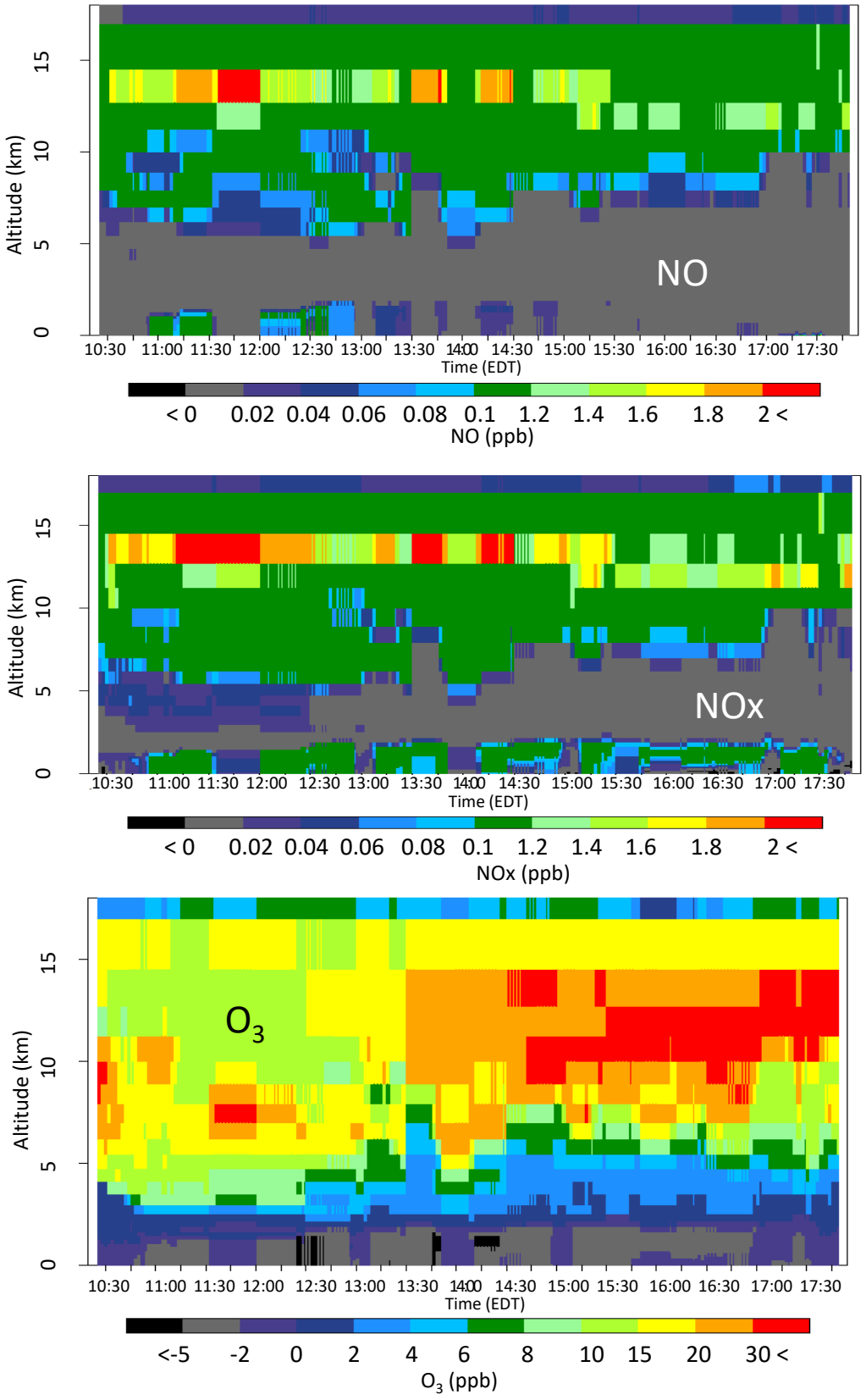

Figure 8. The vertical-time difference between hNLDN and Base during the P3B flight period on July 28, 2011 for (a) NO, (b) NO_X, and (c) O_3.

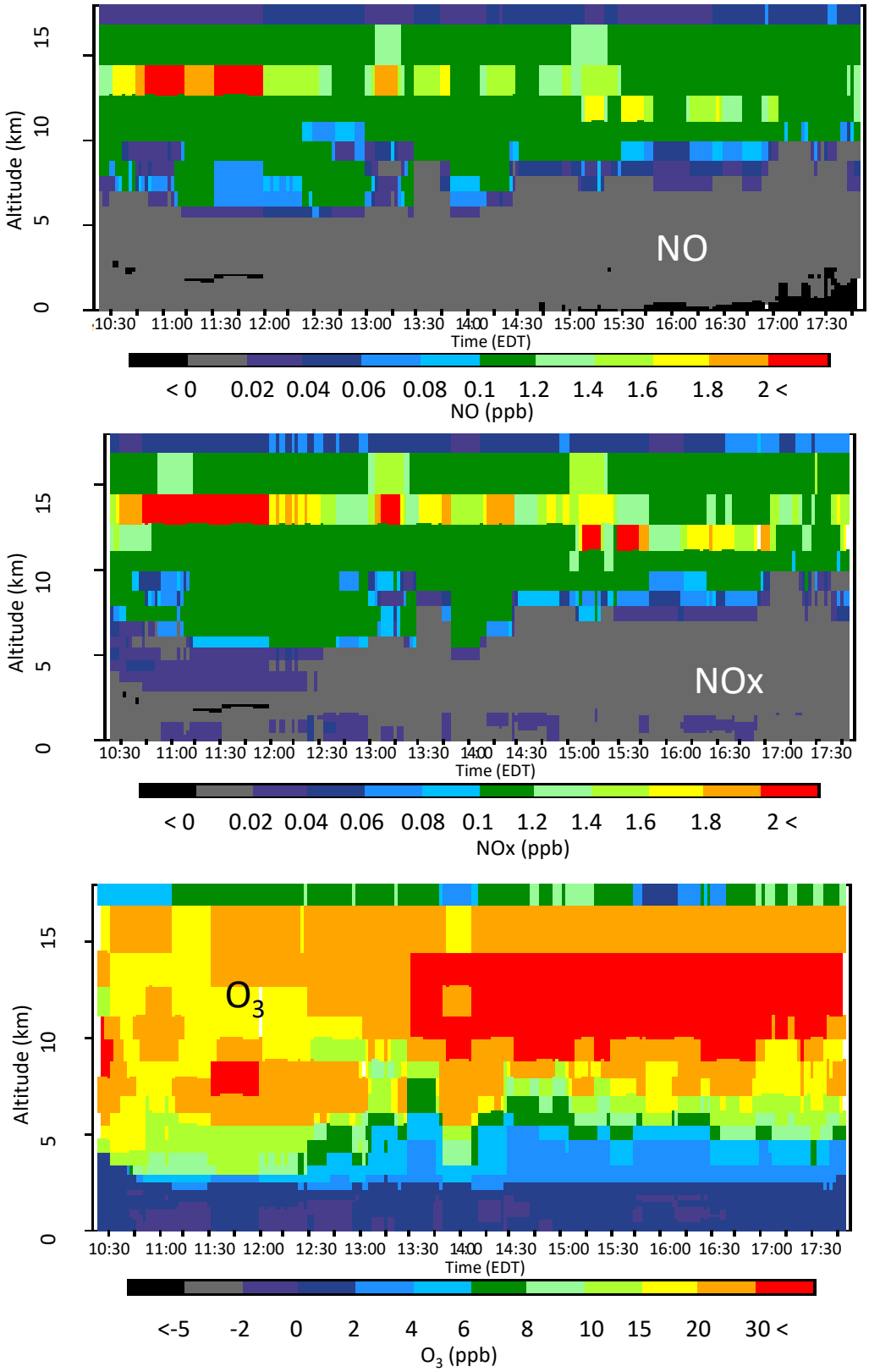

Figure 9. The vertical-time difference between mNLDN and Base during the P3B flight period on July 28, 2011 for (a) NO, (b) NO_X, and (c) O_3.

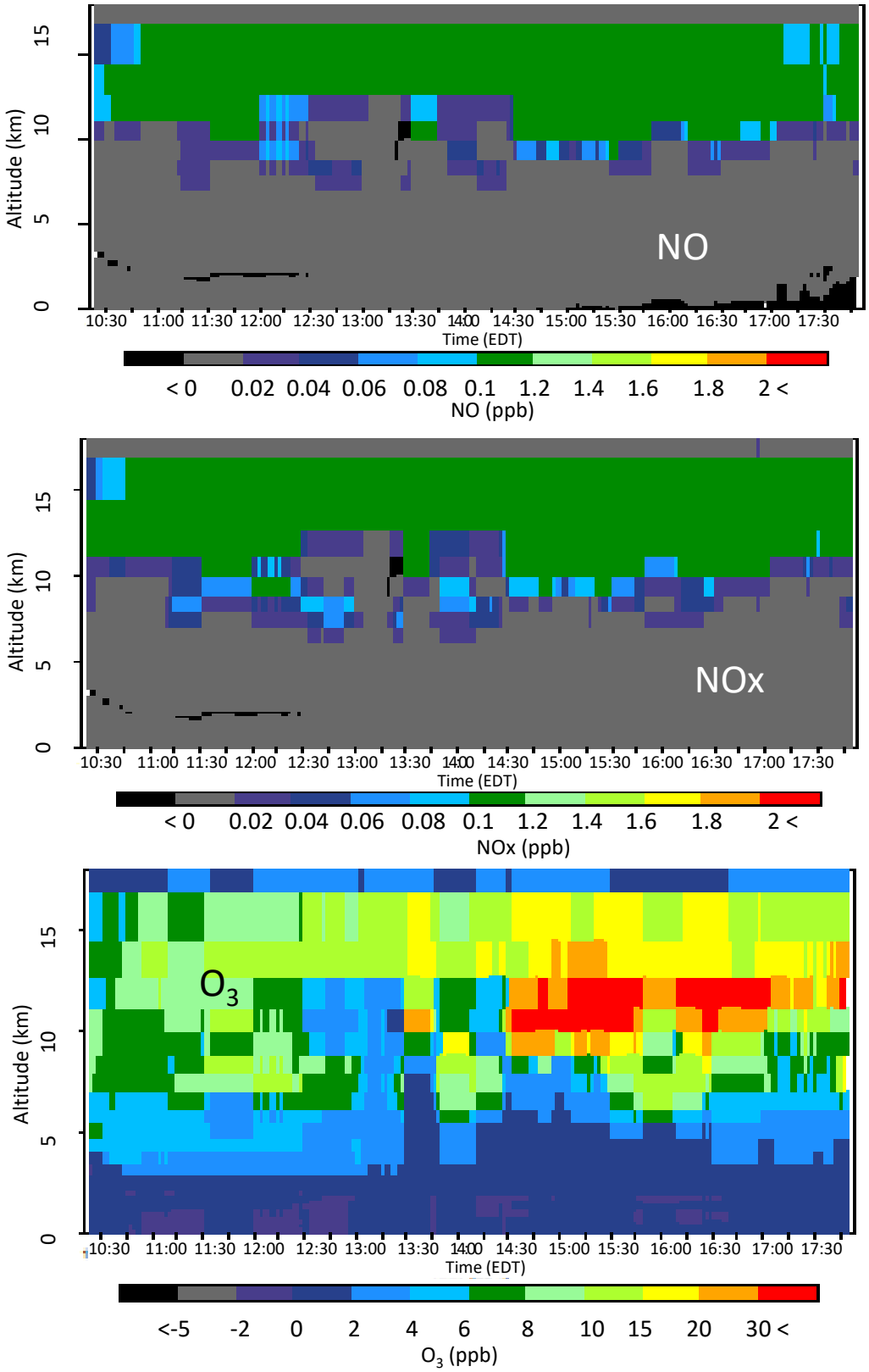

Figure 10. The vertical-time difference between pNLDN and Base during the P3B flight period on July 28, 2011 for (a) NO, (b) NO_X, and (c) O_3.

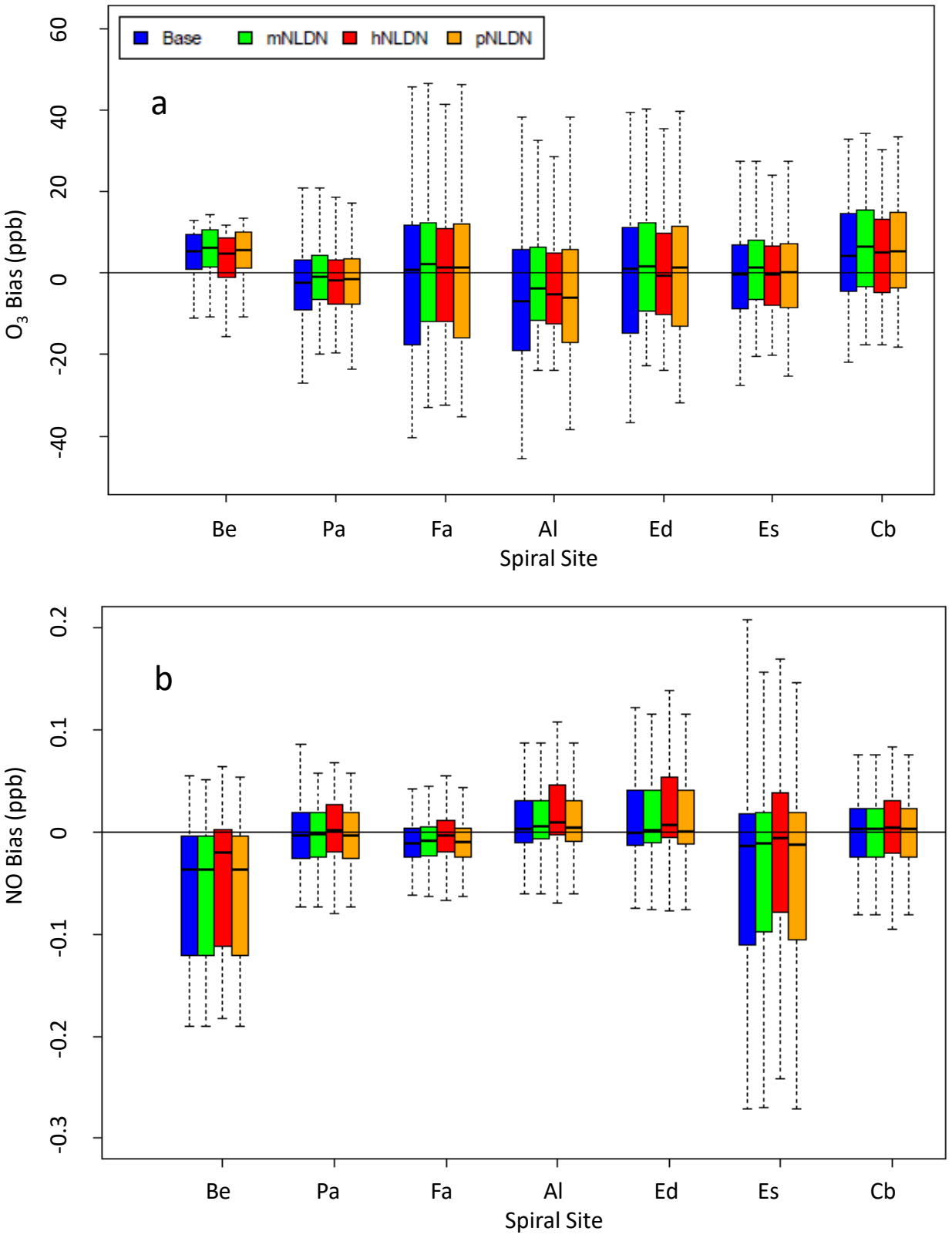

Figure 11. Bias (model – observation) distributions of O_3 (a) and NO (b) at each P3B spiral site on July 21, 22, 28, and 29, 2011. Be: Beltsville, Pa: Padonia, Fa: Fairhill, Al: Aldino, Ed: Edgewood, Es: Essex, Cb: Chesapeake Bay.

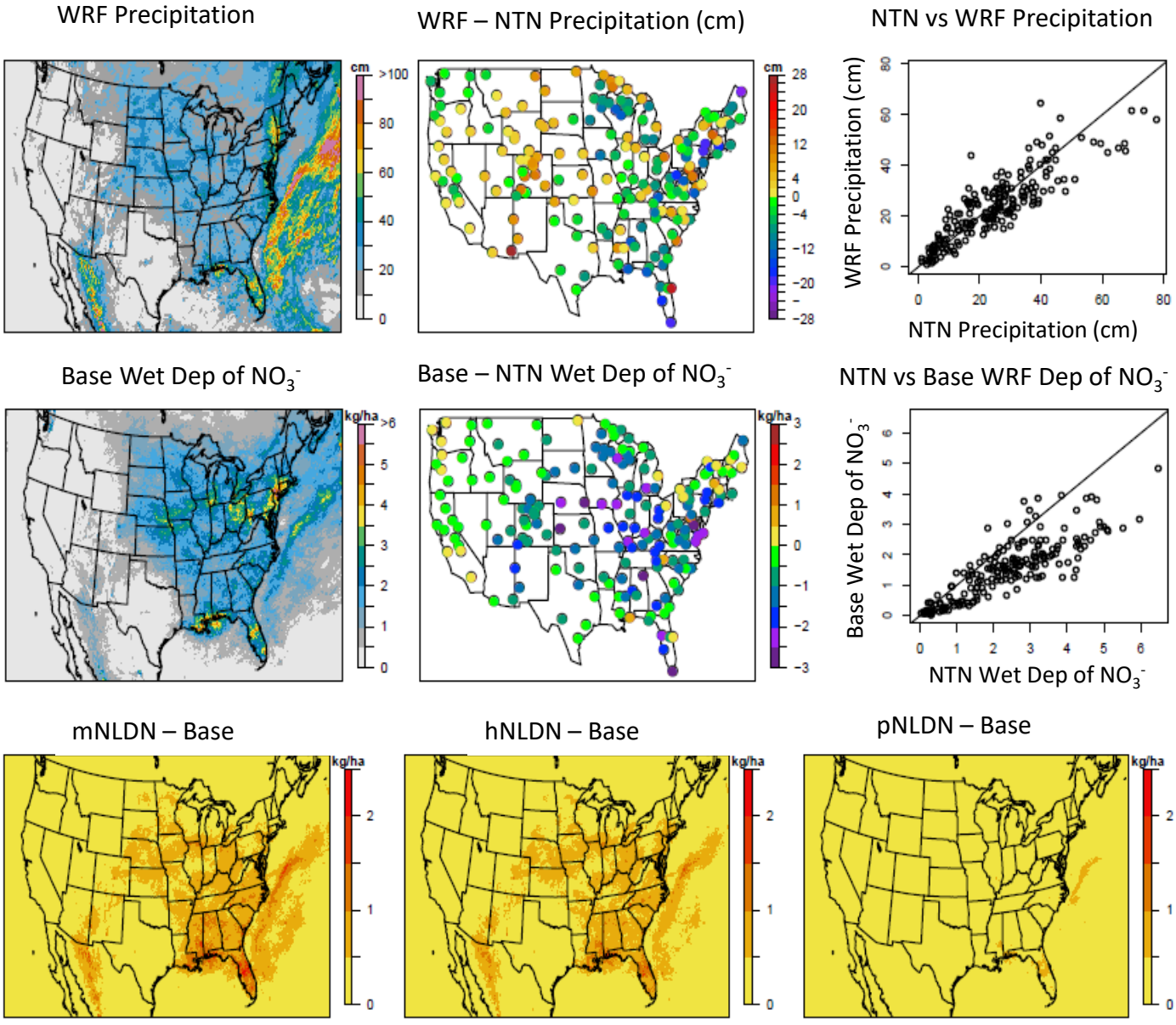

Figure 12. The top row shows precipitation estimates from WRF (left), the bias in the WRF predicted precipitation at NTN locations (middle) , and the corresponding scatter plots (right). The middle row shows wet deposition (Dep) of nitrate estimates from the Base simulation (left), the bias in the Base model estimates of wet deposition of NO_3^- at NADP/NTN locations (middle), and the corresponding scatter plots (right). The bottom row shows the difference in the LNO_X sensitivity simulations and the Base case estimates of wet deposition of NO_3^-: mNLDN – Base (left); hNLDN – Base (middle), and pNLDN – Base (right) . All maps are based on accumulated values (precipitation or wet deposition) during June – August 2011. Precipitation totals are in cm and wet deposition totals are in kg/ha.